Mon. Not. R. Astron. Soc. **308**, 377–404 (1999)

A comparative *HST* imaging study of the host galaxies of radio-quiet quasars, radio-loud quasars and radio galaxies – I

R. J. McLure,[1] M. J. Kukula,[1,2] J. S. Dunlop,[1] S. A. Baum,[2] C. P. O'Dea[2] and D. H. Hughes[2]

[1]*Institute for Astronomy, University of Edinburgh, Blackford Hill, Edinburgh EH9 3HJ*
[2]*Space Telescope Science Institute, 3700 San Martin Drive, Baltimore, MD 21218, USA*

Accepted 1999 March 22. Received 1999 March 22; in original form 1998 October 20

ABSTRACT

We present the first results from a major *HST* WFPC2 imaging study aimed at providing the first statistically meaningful comparison of the morphologies, luminosities, scalelengths and colours of the host galaxies of radio-quiet quasars, radio-loud quasars and radio galaxies. We describe the design of this study and present the images that have been obtained for the first half of our 33-source sample. We find that the hosts of all three classes of luminous AGN are massive elliptical galaxies, with scalelengths $\simeq$10 kpc, and $R-K$ colours consistent with mature stellar populations. Most importantly, this is first unambiguous evidence that, just like radio-loud quasars, essentially all radio-quiet quasars brighter than $M_R = -24$ reside in massive ellipticals. This result removes the possibility that radio 'loudness' is directly linked to host galaxy morphology, but is however in excellent accord with the black hole/spheroid mass correlation recently highlighted by Magorrian et al. We apply the relations given by Magorrian et al. to infer the expected Eddington luminosity of the putative black hole at the centre of each of the spheroidal host galaxies we have uncovered. Comparison with the actual nuclear *R*-band luminosities suggests that the black holes in most of these galaxies are radiating at a few per cent of the Eddington luminosity; the brightest host galaxies in our low-z sample are capable of hosting quasars with $M_R \simeq -28$, comparable to the most luminous quasars at $z \simeq 3$. Finally, we discuss our host-derived black hole masses in the context of the radio luminosity:black hole mass correlation recently uncovered for nearby galaxies by Franceschini et al., and consider the resulting implications for the physical origin of radio loudness.

Key words: black hole physics – galaxies: active – galaxies: photometry – quasars: general – infrared: galaxies.

1 INTRODUCTION

Studies of the host galaxies of active galactic nuclei (AGN) may hold the key to answering several important questions about these still poorly understood objects. Such questions include (i) what is the physical origin of radio loudness?, (ii) by what mechanisms are galactic nuclei triggered into activity (e.g. Smith & Heckman 1990; Hutchings & Neff 1992)?, (iii) which classes of AGN can be unified via orientation effects (Peacock 1987; Barthel 1989; Urry & Padovani 1995)?, (iv) which classes of AGN can or cannot be unified via time evolution (e.g. Ellingson, Yee & Green 1991), and (v) how does the recently inferred relation between black hole mass and galaxy bulge mass (Magorrian et al. 1998) extend to high masses? Furthermore, by defining the parameter space occupied by AGN hosts, important constraints can be derived on the fraction of the galaxy population which might contain a dormant AGN, constraints which need to be satisfied by any physical model which endeavours to explain the cosmological evolution of active galaxy populations (Small & Blandford 1992; Haehnelt & Rees 1993; Dunlop 1997; Silk & Rees 1999).

Determining the properties of the hosts of relatively low-luminosity AGN such as Seyfert nuclei has proved relatively straightforward since the advent of CCD detectors, and their properties are now reasonably well established (e.g. MacKenty 1990). However, studying the properties of quasar host galaxies presents a far more serious challenge due to the combination of their larger cosmological distances, and much higher nuclear:host luminosity ratios. Initial attempts to image quasar hosts from the ground did achieve a limited degree of success and led to a reassessment of long-held views and suppositions about galaxies

with powerful nuclear activity (e.g. Smith et al. 1986; Véron-Cetty & Woltjer 1990). In particular, they overturned the notion (arrived at by analogy with Seyferts) that radio-quiet quasars would be found only in spiral galaxies (e.g. Véron-Cetty, Woltjer & Roy 1991). However, the potential of ground-based observations of quasar hosts is fundamentally limited by atmospheric seeing, and effective *optical* studies have generally proved to be extremely difficult to carry out from the ground. This is unfortunate, because a clear understanding of both the differences and similarities between the host galaxies of the three main classes of *powerful* active galaxy – radio-quiet quasars (RQQs), radio-loud quasars (RLQs) and radio galaxies (RGs) – is obviously of fundamental importance in any attempt to unify or relate the various manifestations of the AGN phenomenon.

One way to reduce the distorting influence of the nuclear light is to observe at near-infrared (NIR) wavelengths where the nuclear:host luminosity ratio can be minimized (Dunlop et al. 1993). The advantages of this approach are demonstrated to good effect by McLeod & Rieke (1994a,b), who observed a sample of Seyfert galaxies and nearby quasars in the *H* band and found that, despite the large scatter in host properties for AGN of low luminosity, for high-luminosity quasars there appears to be a minimum host *H*-band luminosity which increases with nuclear power (McLeod & Rieke 1995a). Successful NIR imaging of quasar hosts has also been carried out by Kotilainen & Ward (1994), Hutchings & Neff (1997) and Carballo et al. (1998).

We have also exploited this fact, while at the same time attempting to minimize cosmological distance, via an extensive *K*-band imaging study of the hosts of matched samples of RQQs, RLQs and RGs in the redshift range $0.1 \leq z < 0.35$ (Dunlop et al. 1993; Taylor et al. 1996). This infrared study was successful in that, unlike previous ground-based optical studies, it proved possible to determine reliably the morphological type of a substantial fraction (>0.5) of the quasar hosts. Moreover, the use of properly matched samples allowed us to demonstrate that the hosts of all three classes of powerful AGN were large (≥ 10 kpc), luminous ($> 2L^*$) galaxies, and that the hosts of RLQs and RGs were statistically identical, consistent with unified models. We also found that at least some of the RQQs appeared to lie in elliptical rather than disc-like galaxies, and there was a suggestion in our data that the probability of an RQQ having an elliptical host is an increasing function of quasar luminosity (a tendency also noted by McLeod & Rieke 1995b). However, we were unable to prove that this effect was significant, due to the fact that the morphologies of the hosts of the more luminous RQQs in our sample remained ambiguous with the limitations of ground-based seeing. This drawback, coupled with the desirability of obtaining reliable optical–infrared colours for all the host galaxies in our AGN sample led us to undertake a complementary *R*-band imaging study of this same sample with WFPC2 on the *HST*. Here we report the first results of this, the most detailed *HST* study to date of the host galaxies of quasars and radio galaxies.

While the observed nuclear:host luminosity ratio of a quasar is inevitably much higher at *R* than at *K*, the high spatial resolution offered by *HST* allows the nuclear contamination to be confined to the central regions of the host galaxy image, thus enhancing the prospects of reliable determination of host galaxy morphology, luminosity and scalelength. This resolution advantage has previously been explored in a number of pilot *HST* studies of small samples of quasars (Bahcall, Kirkhados & Schneider 1994, 1995a,b,c; Hutchings et al. 1994; Disney et al. 1995; Hutchings & Morris 1995), although it comes with the price that the nucleus inevitably saturates in any *HST* image of sufficient depth to produce a useful image of the underlying host. As a result, it has proved difficult to perform accurate subtraction of the nuclear contribution, which is still vitally important for the reliable determination of host galaxy properties (Hutchings 1995). A second problem with some previous *HST* studies has been the use of filters which have included strong emission lines, making it difficult to discern which host galaxy features can be reliably attributed to starlight (Bahcall et al. 1995a). A third problem has been the use of the wide *V*-band filter, which fails to sample properly the dominant stellar population of the host (at $\lambda_{\rm rest} > 4000$ Å) for $z > 0.25$ (Bahcall et al. 1994). A fourth problem has been the unavailability of an accurate point spread function (PSF) of sufficient depth to investigate the contribution of the quasar nucleus at large radii (>3 arcsec) due to the problem of scattered light within WFPC2.

As described in more detail below, our new 34-orbit *HST R*-band study of the hosts of RQQs, RLQs and RGs has been designed to overcome these problems, and it differs from previous *HST* studies of quasar hosts in five important ways. First, we are imaging statistically comparable samples of each class of AGN. Second, we already possess deep infrared images of all our targets, which will allow the first meaningful study of the optical–infrared colours of quasar hosts. Third, we have used the F675W *R*-band filter, and restricted the redshift range of our targets, in order to ensure that the images are always uncontaminated by emission lines, and we always sample the rest frame emission of the host galaxy longward of the 4000-Å break. Fourth, we have devoted an orbit of our *HST* observing programme to assembling an accurate PSF of sufficient dynamic range to define accurately the contribution of the quasar nucleus out to an angular radius $r > 10$ arcsec. Fifth, we have developed and applied a two-dimensional modelling procedure which allows us to extract reliably the morphology, luminosity and size of the host galaxies from our images, without requiring us to make asumptions a priori about the values of these parameters (which contrasts with the analysis of Bahcall et al. 1994 as highlighted by McLeod & Rieke 1995b and Bahcall et al. 1997).

The results presented here from the first year of this study demonstrate the importance of these five improvements. In particular, whereas most previous *HST* studies have tended to highlight the fact that many quasar hosts display a wide range of morphological peculiarities, our study is already revealing a surprising degree of similarity and homogeneity in the spatial distribution and age of the dominant stellar populations in the hosts of these powerful AGN.

The layout of the paper is as follows. In Section 2 we summarize the main properties of the matched RG, RLQ and RQQ samples which are the subject of this *HST* study, and then in Section 3 we give details of the observations, image reduction and PSF determination. In Section 4 we present the images, list and summarize the results of applying our host-galaxy modelling procedure to these data, and provide brief notes on the images of each of the 19 AGN observed to date in the context of previous observations. In Section 5 we discuss the main implications of the trends uncovered by the initial results of this study, and in Section 6 we summarize our principal conclusions. Unless otherwise stated, $\Omega_0 = 1$ and $H_0 = 50\,{\rm km\,s^{-1}\,Mpc^{-1}}$ are assumed throughout, and we convert previously published scalelengths and luminosities to this cosmology for ease of comparison.

2 THE SAMPLE

The full sample selected for *HST* imaging consists of 33 objects (10 RLQs, 13 RQQs and 10 RGs) selected from the slightly larger statistically matched samples which were imaged in the NIR by Dunlop et al. (1993) and Taylor et al. (1996). Full details of these samples can be found in these papers. The key point is that the RLQ and RQQ subsamples were selected to be statistically indistinguishable in terms of optical luminosity and redshift, while the RLQ and RG subsamples were selected to be indistinguishable in terms of radio luminosity, radio spectral index and redshift. Note that, following the radio observations of Kukula et al. (1998), we now possess either a radio detection or a strong upper limit on radio luminosity for all the RQQs in our sample, making it possible to quantify their 'radio quietness', and hence explore the extent to which this can be related to any properties of the host galaxy (see Section 5).

The original combined sample comprised a total of 40 objects (12 RGs, 13 RLQs and 15 RQQs) with $0.1 < z < 0.35$, but for this *HST* study we have restricted the redshift range in order to avoid [O III] emission entering the blue end of the F675W filter. This results in the slightly smaller subsamples described above, without compromising their statistical compatibility. The 19 objects which have been observed during the first year of this study, and for which we present the data in this first paper, are listed in Table 1, along with the dates on which they were observed with the *HST*.

3 OBSERVATIONS

3.1 Detector and filter choice

Observations were made with the Wide Field & Planetary Camera 2 (WFPC2) (Trauger et al. 1994) on the *Hubble Space Telescope* (*HST*) using the F675W filter. The filter spans 877 Å in the wavelength range 6275.5–7152.5 Å, roughly equivalent to standard *R* band, and thus excludes both [O III] λ5007 and Hα emission for redshifts $0.1 \leq z \leq 0.25$ (a wider filter, though providing greater throughput, would have allowed our images to become contaminated by line emission which could mask, or at least be confused with, the underlying stellar continuum of the host galaxy).

WFPC2 consists of four detectors, each comprising 800×800 pixels: three WF chips, each with a pixel scale of 100 mas; and one PC chip, with a pixel scale of 45 mas. Although the PC chip offers smaller pixels and correspondingly better sampling of the instrument PSF, it is ultimately less sensitive to low-surface-brightness emission than the WF chips, even when the pixels are binned up, and we therefore opted to use the larger detectors. Target sources were centred on the WF2 chip, which was chosen for its marginally better performance over the period immediately prior to our observations.

Table 1. Observing dates for the objects presented in this paper.

Object	*HST* Archive designation	Type	Observing date
GRW+70D5824	PSF-STAR	STAR	Aug 07 1997
0958+291	3C234.0	RG	Jun 11 1997
0345+337	3C93.1	RG	Feb 16 1998
0917+459	3C219	RG	Mar 25 1998
2141+279	3C436	RG	Apr 27 1998
2247+140	PKS2247+14	RLQ	Jun 25 1997
2141+175	OX169	RLQ	Jul 01 1997
0137+012	PHL1093	RLQ	Jul 04 1997
2349−014	PKS2349−01	RLQ	Jul 05 1997
1004+130	PKS1004+13	RLQ	Nov 28 1997
0736+017	PKS0736+01	RLQ	Feb 06 1998
0953+415	PG0953+415	RQQ	Jun 02 1997
0054+144	PHL909	RQQ	Jun 27 1997
2344+184	2344+184	RQQ	Jun 28 1997
0244+194	0244+194	RQQ	Jun 29 1997
0157+001	0157+001	RQQ	Jun 30 1997
0257+024	US3498	RQQ	Jul 04 1997
1635+119	MC1635+119	RQQ	Feb 19 1998
0923+201	PG0923+201	RQQ	Mar 12 1998
1012+008	PG1012+00	RQQ	Mar 12 1998

3.2 Observing strategy and image reduction

Observations of the target quasars and radio galaxies were carefully tailored to ensure that the maximum amount of information could be derived from the final images. In both cases, deep, sensitive images of the galaxies are clearly desirable, but for the quasars such exposure times inevitably entail saturation of the central source, allowing no independent measure of PSF normalization.

Slightly different strategies were therefore used for the quasar and radio galaxy samples. For the quasars, exposures of 5, 26 and 3×600 s were taken. The short exposures guaranteed that at least one unsaturated image of the quasar would be obtained, thus ensuring an accurate measure of the central flux density. The three 600-s exposures each provided a 3σ surface-brightness sensitivity $\mu_R = 23.8\,\mathrm{mag\,arcsec^{-2}}$ (per pixel), and their comparison facilitated reliable cosmic ray removal using standard IRAF tasks. With azimuthal averaging, the combined 1800-s deep image of each quasar allows extended emission to be traced reliably out to a surface brightness level $\mu_R > 26\,\mathrm{mag\,arcsec^{-2}}$.

For the radio galaxies there was little danger of saturation, and so short exposures were not required. Three 700-s exposures were therefore obtained for each radio galaxy. Any remaining time in the orbit was filled with an exposure of flexible length (usually 40 to 100 s).

The sources discussed in this paper – constituting approximately half of our sample – were all observed between 1997 June and 1998 April (see Table 1 for exact dates). Calibration was carried out using the standard pipeline.

3.3 Determining the point spread function

The form of the WFPC2 point spread function (PSF) depends critically on both the position on the chip and the spectral energy distribution (SED) of the target source. These effects are well understood and can be included in software to produce accurate synthetic PSFs. However, despite providing an excellent fit over the central few arcseconds, the synthetic PSFs produced by packages such as TINYTIM deviate from the empirical WFPC2 PSF at larger radii ($\geq$2 arsec). This is due to scattering within the camera. Since the scattered light shows complex structure which is not uniform, and which is also wavelength- and position-dependent, it cannot easily be modelled.

We therefore devoted one orbit of our allotted *HST* time to constructing a deep, unsaturated stellar PSF using the F675W

filter, with the star centred on exactly the same part of the WF2 chip as the target objects.

The star chosen was GRW +70D5824, a white dwarf of spectral type DA3 and apparent magnitude $V = 12.77$. Since it also serves as a UV standard star for WFPC2, the position and spectrum of this object are extremely well determined (Turnshek et al. 1990). No stars of a comparable brightness lie within 30 arcsec, ensuring that the stellar PSF is not contaminated by PSFs or scattered light from neighbouring objects. The $B-V$ colour of the PSF star is 0.09, sufficiently similar to the neutral colours ($B-V \simeq 0$) typical of our quasar sample to provide a reasonable match to a quasar SED over the wavelength range of the F675W filter.

In order to obtain both unsaturated images of the PSF core *and* deep images of the wings, a series of exposures was carried out with durations of 0.23, 2, 26 and 160 s. After 0.23 s the central pixel of the stellar image reaches approximately 10 per cent of its saturation value (assuming that the star is perfectly centred). This is the shortest practical exposure length – in exposures of less than 0.23 s the PSF would be compromised by the shutter flight time. Subsequent exposure durations were carefully staggered to ensure that the star never saturated beyond the radius at which the wings of the PSF in the previous, shorter exposure became lost in the noise. This allowed us to build up a composite PSF of very high dynamic range by splicing together annuli from successively deeper exposures.

The brightest quasar in our sample has an apparent magnitude of $V = 15.15$, more than 2 mag fainter than the PSF star. We were therefore able to ensure that the deepest stellar image probed much further into the wings of the PSF than even the longest quasar exposure.

Each exposure also used a two-point dither pattern to improve the sampling of the PSF (which is significantly undersampled by the 0.1-arcsec pixel scale of the WF chips).

Thus the stellar PSF is designed to match the PSFs of the target quasars as closely as possible in terms of depth, position on the detector, and SED. However, we note that we cannot account for time-dependent variations in the PSF using this method. These variations are due to changes in the telescope focus and include contributions from several sources. Of these, the most significant for our observations is the short-term (intra-orbit) variability ('breathing') due to temperature fluctuations in the telescope's environment. However, with the relatively large pixel scale of the WF chips the effect on the amount of flux falling on the central pixel of a point source is likely to be only a few per cent at most.

4 RESULTS

4.1 Images

The images, two-dimensional model fits, and model-subtracted residual images are presented in Appendix A in Figs A1–A19. A grey-scale/contour image of the final reduced F675W *R*-band image of each AGN is shown in the top-left panel (panel A) of each Fig. A1–A19, which shows a region 12.5×12.5 arcsec^2 centred on the target source. The surface brightness of the lowest contour level is indicated in the top-right corner of the panel, with the grey-scale designed to highlight structure close to this limit. Higher surface-brightness contours are spaced at intervals of 0.5 mag arcsec^{-2}, and have been superimposed to emphasize brighter structure in the centre of the galaxy/quasar. Panel B of each figure shows the best-fitting two-dimensional model, complete with unresolved nuclear component (after convolution with the empirical PSF) contoured in an identical manner to panel A. Panel C shows the best-fitting host galaxy as it would appear if the nuclear component were absent, while panel D is the residual image which results from subtraction of the full two-dimensional model (in panel B) from the raw *R*-band image (in panel A), in order to highlight the presence of morphological peculiarities such as tidal tails, interacting companion galaxies, or secondary nuclei. All panels are displayed using the same grey-scale.

4.2 Modelling results

Full details of the two-dimensional modelling procedure which we have used to determine the properties of the host galaxies are presented elsewhere, along with the results of extensive tests of its ability to reclaim the true properties of a wide range of host-galaxy:nucleus combinations at different redshifts (McLure et al. 1999). In brief, the modelling procedure is a development of that used by Taylor et al. (1996), and here we have used two distinct versions of this procedure to determine the host-galaxy properties from our *HST* images. For both versions an accurate high-dynamic-range PSF and an accurate error frame for each quasar image are essential for the extracton of robust results (see McLure et al. for details).

In the first version the host-galaxy morphology is constrained by determining how well the data can be reproduced *assuming* that the host galaxy is *either* an elliptical galaxy (described by a de Vaucouleurs $r^{1/4}$ law) or an exponential disc. The remaining five parameters (host-galaxy position angle, host-galaxy axial ratio, host-galaxy scalelength, host-galaxy luminosity and nuclear luminosity) are then varied until, when convolved with the PSF, the model best fits the data as determined by χ-squared minimization (note that it is not assumed a priori that the radio galaxies have a negligible nuclear component). Then, if one assumed galaxy morphology yields a significantly better fit than the other, we can say that the galaxy is *better* described by a de Vaucouleurs law or by an exponential disc. The results of applying this procedure to the *HST* images are given in Table 2. The striking feature of these results is that all of the host galaxies except those of the two lowest luminosity RQQs are better described as elliptical galaxies, and that, with only one exception (the heavily nuclear dominated RQQ 0953+415), this difference is statistically very significant. One-dimensional luminosity profiles extracted from the best-fitting de Vaucouleurs or exponential models are compared with the data in Fig. 1.

In the second version we have removed the need to assume that the host galaxy can be described by either a pure $r^{1/4}$ law or exponential disc, and allow a sixth parameter β [where the luminosity profile of the galaxy is given by $I(r) \propto \exp(-r^{\beta})$] to vary continuously. Thus, $\beta = 1$ should result if the galaxy is best described by a pure exponential disc, and $\beta = 0.25$ should result if the galaxy really does follow a pure de Vaucouleurs law, but *all* values of β are available to the program to improve the quality of the model fit. The impressive results of applying this procedure to the *HST* images are given in Table 3 and illustrated in Fig. 2. One remarkable feature of these results (see Fig. 2) is that for 16 out of the 19 objects, the preferred β parameter for the host galaxy is in the range $0.18 < \beta < 0.3$, in excellent agreement with a pure de Vaucouleurs law. Perhaps most surprisingly, given pre-existing prejudices, this is true for six out of the nine RQQs in the current

Table 2. The outcome of attempting to model the AGN host galaxies as either an exponential disc or a de Vaucouleurs spheroid. The preferred host-galaxy morphology is given in column 2, with the $\Delta\chi^2$ between the chosen and alternative model given in column 3. In column 4, $r_{1/2}$ is given irrespective of the chosen host morphology. Column 5 lists $\mu_{1/2}$ in units of R mag arcsec^{-2}. Columns 6 and 7 list the integrated apparent magnitudes of the host galaxy and fitted nuclear component converted from F675W to Cousins R band, while column 8 gives the ratio of integrated galaxy and nuclear luminosities. Columns 9 and 10 give the axial ratio and position angle of the best-fitting host respectively.

Source	Host	$\Delta\chi^2$	$r_{1/2}$/kpc	$\mu_{1/2}$	$R_{\rm host}$	$R_{\rm nuc}$	$L_{\rm nuc}/L_{\rm host}$	b/a	PA/°
RG									
0345+337	Elliptical	2349	11.0	23.1	18.0	21.1	0.06	0.70	99
0917+459	Elliptical	33245	19.1	23.0	16.1	19.4	0.05	0.76	36
0958+291	Elliptical	7793	8.3	22.0	17.1	18.5	0.27	0.95	45
2141+279	Elliptical	8530	21.3	23.4	16.7	25.6	0.0003	0.74	148
RLQ									
0137+012	Elliptical	5093	13.1	22.6	17.2	17.3	0.8	0.85	35
0736+017	Elliptical	8909	13.3	22.9	16.9	16.2	1.9	0.97	13
1004+130	Elliptical	501	8.2	21.5	16.9	15.0	5.8	0.94	29
2141+175	Elliptical	1381	3.7	20.3	17.2	16.0	3.2	0.55	118
2247+140	Elliptical	8092	10.7	22.4	17.2	16.9	1.3	0.63	118
2349−014	Elliptical	13463	18.1	22.7	15.9	16.0	0.9	0.89	45
RQQ									
0054+144	Elliptical	6050	8.1	21.7	16.6	15.5	2.7	0.61	108
0157+001	Elliptical	12826	7.9	20.9	15.8	16.2	0.72	0.83	97
0244+194	Elliptical	2744	8.9	22.7	17.5	16.8	1.9	0.92	77
0257+024	Disc	15361	10.1	21.5	15.9	19.5	0.04	0.89	134
0923+201	Elliptical	1733	8.2	22.1	17.2	15.7	4.2	0.98	141
0953+415	Elliptical	91	7.1	22.4	18.2	15.2	15.4	0.86	115
1012+008	Elliptical	1056	23.0	23.8	16.6	16.2	1.5	0.64	109
1635+119	Elliptical	34765	6.3	21.6	16.8	18.1	0.3	0.69	179
2344+184	Disc	22348	8.8	22.7	17.2	19.2	0.2	0.79	146

subsample. Moreover, the only two RQQs which appear to have a significant disc component are the two least-luminous RQQs in this subsample. The clear implication is that *all* bright quasars, with $M_R < -23.5$ reside in massive ellipticals, irrespective of their radio power. Such a result has been hinted at before (Disney et al. 1995; Taylor et al. 1996), but this is the first time it has proved possible to demonstrate unambiguously that this is the case.

4.3 Notes about individual objects

Here we provide a brief discussion of the *HST* image of each object presented in this paper, with reference to other recent *HST* and ground-based data. A more detailed description of each object, together with our existing *K*-band images, can be found in Dunlop et al. (1993) and Taylor et al. (1996). Sources are listed by IAU name, with alternative names given in parenthesis. Radio luminosities or upper limits at 5-GHz have been calculated assuming $H_0 = 50\,{\rm km\,s^{-1}\,Mpc^{-1}}$ and $\Omega_0 = 1$. Note that following the deep VLA radio observations of RQQs undertaken by Kukula et al. (1998), radio detections or strong upper limits are now available for all the RQQs in the current sample.

4.3.1 The radio galaxies

0345+337 (3C 93.1, 4C +33.08, B2 0345+33, NRAO 0146, DA 113, OE +376)

$[z = 0.244,\ \log_{10}(L_{5\,\rm GHz}/{\rm W\,Hz^{-1}\,sr^{-1}}) = 25.45]$

The results of our modelling of this object, shown in Fig. A1, reveal the host to be a large elliptical galaxy, with $r_{1/2} = 11$ kpc. The strong preference for a elliptical host is confirmed by the variable-beta modelling, which yields $\beta = 0.249$. The unresolved central point source is weak, making up ≈6 per cent of the integrated flux in the best-fitting model. The model-subtracted image shows some low-level residual flux unaccounted for by the symmetrical host template.

The embedded companion detected 6 arcsec NW of the main galaxy in our *K*-band image is seen as clearly separated in the new *R*-band image. The other companion detected to the SE at *K* is again detected here, together with several other faint companion objects. The two steep-isophote companions are confirmed to be foreground stars from our *HST* image.

At high resolution in the radio this is a compact steep-spectrum source having a diameter of ≃ 0.4 arcsec (Akujor et al. 1991).

0917+459 (3C 219, 4C +45.19, NRAO 0320, DA 266, LHE 249, OK +430)

$[z = 0.174,\ \log_{10}(L_{5\,\rm GHz}/{\rm W\,Hz^{-1}\,sr^{-1}}) = 25.69]$

A disc host for this radio galaxy is excluded by our model fitting with a high level of confidence. As shown in Figs A2 and 1(b), the host is a large elliptical, $r_{1/2} = 19$ kpc, with a very weak, unresolved nuclear component. The variable-beta model again chooses an almost perfect de Vaucouleurs template, with $\beta = 0.229$. This galaxy has been recently imaged with *HST* in a snapshot survey of 3CR radio galaxies (De Koff et al. 1996), through the F702W (wide *R*) filter. De Koff et al. suggest that there may be an interaction with the large galaxy to the SE. However, our model-subtracted image provides little direct evidence for any interaction.

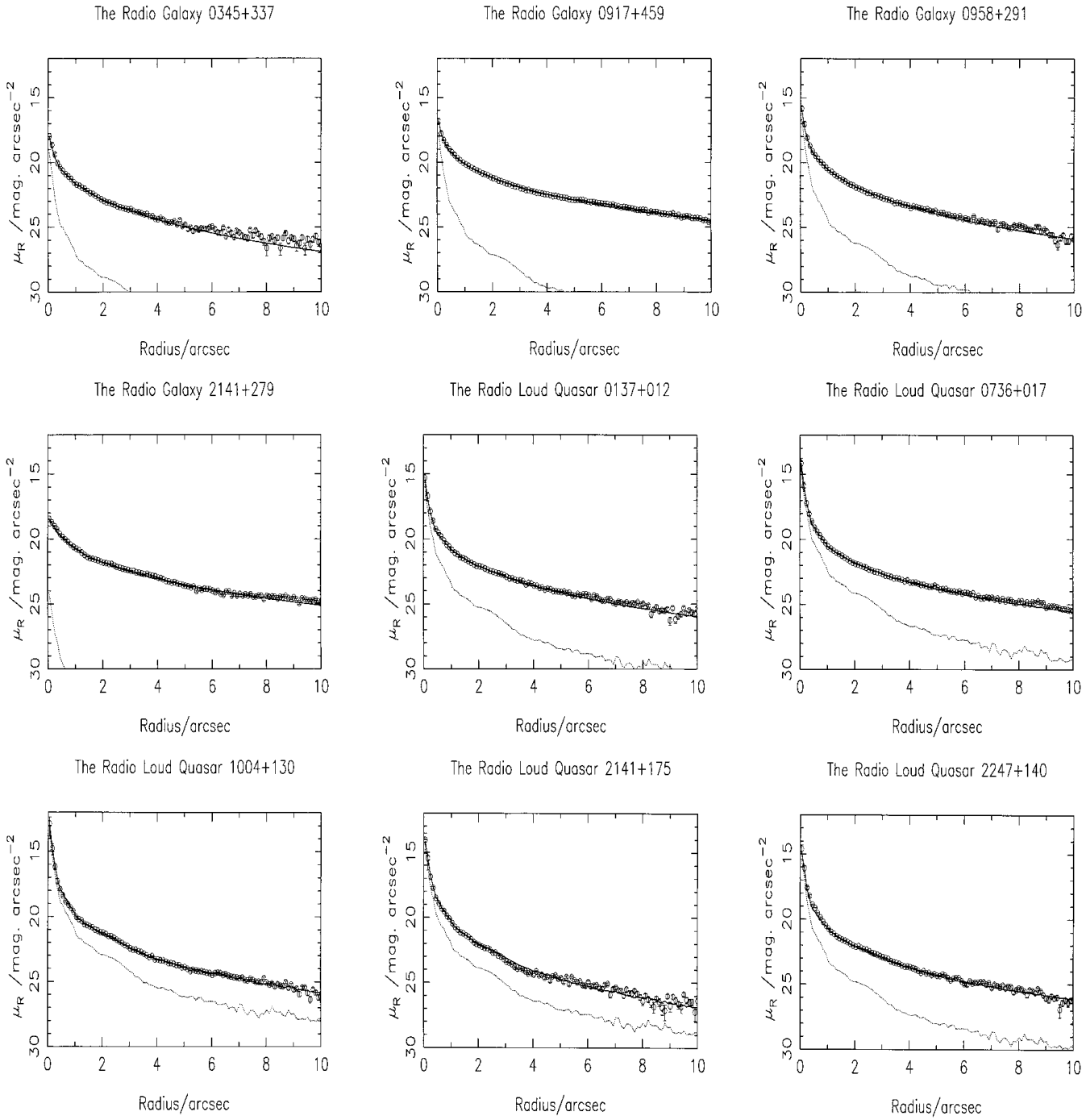

Figure 1. A comparison of the azimuthally averaged luminosity profiles derived from the images with those produced by the two-dimensional modelling. Each plot shows the azimuthally averaged image data (open circles), the azimuthally averaged best-fitting model after convolution with the PSF (solid line) and the azimuthally averaged best-fitting unresolved nuclear component after convolution with the PSF (dotted line).

This galaxy is clearly situated in a cluster, with a large number of companion objects detected at *R* and in our previous *K*-band image. In the radio this is a classical double source whose position angle is anticorrelated with the optical and NIR position angles.

0958+291 (3C 234.0, 4C +29.35, IRAS F09589+2901, B2 0958+29, NRAO 0343, CSO 0031, OL +200, DA 280, CTD 064, CTA 049)

[$z = 0.185$, $\log_{10}(L_{5\,\mathrm{GHz}}/\mathrm{W\,Hz^{-1}\,sr^{-1}}) = 25.30$]

As shown in Figs A3 and 1(c), the host is extremely well fitted by an elliptical galaxy template, with $r_{1/2} = 8.3$ kpc, and a disc host is formally excluded. This result is supported by the variable-beta model, which yields another virtually perfect de Vaucouleurs model ($\beta = 0.253$). This galaxy has a rather more luminous unresolved component, which contributes nearly 30 per cent of the integrated flux. 3C 234.0 was also included in the *HST* snapshot survey (De Koff et al. 1996), where features were detected emanating to the east and west of the galaxy nucleus. The large tidal arm

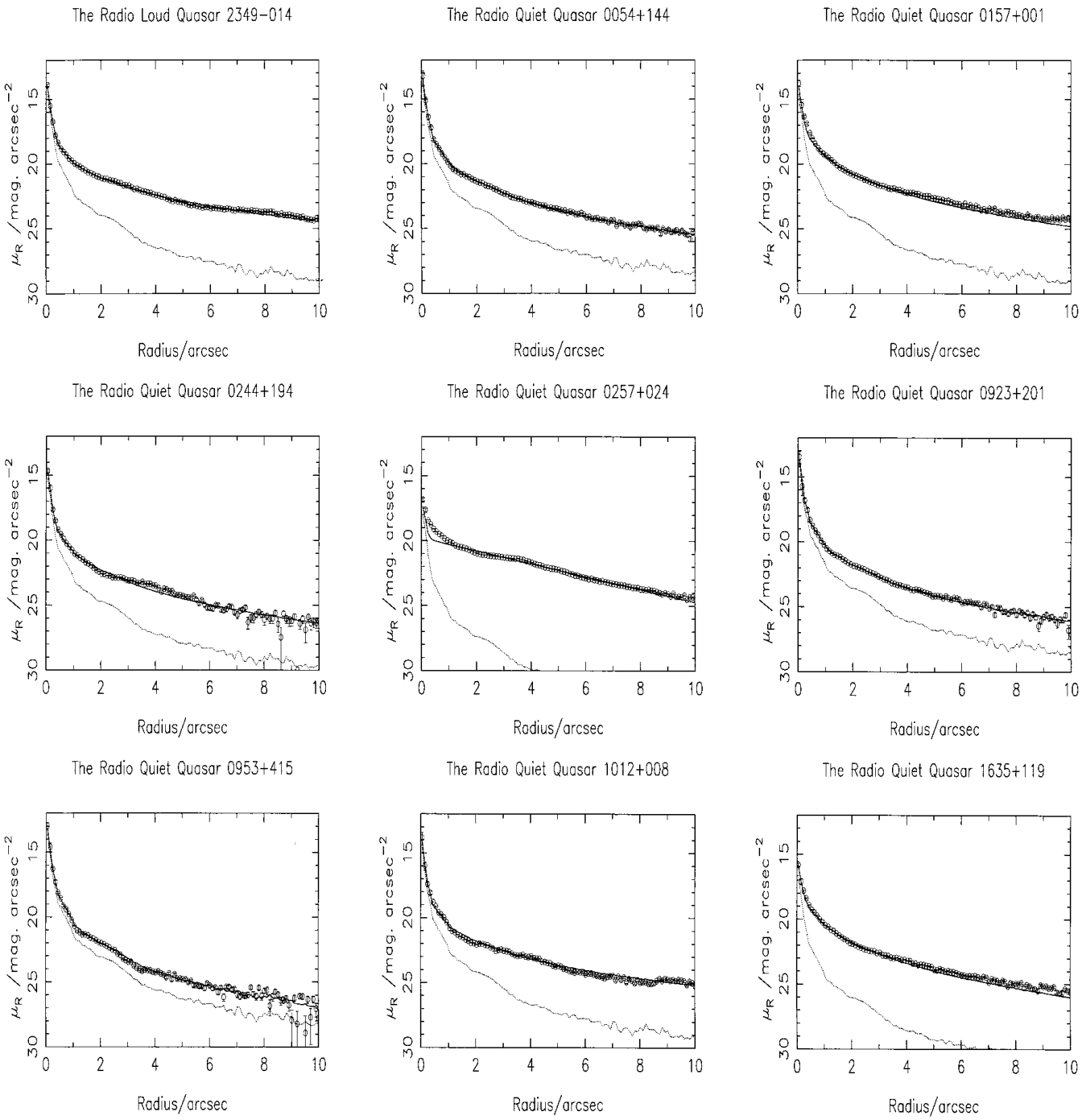

Figure 1 – *continued*

to the west of the nucleus is easily visible in the contour plot in Fig. A3, and is dramatically highlighted in the model-subtracted image. A fainter counterarm to the east of the nucleus is also present, although it is not easily discerned in this grey-scale image.

Numerous companion objects are detected in our *R*-band image, in agreement with the ground-based images of Hutchings, Johnson & Pyke (1988) through the same filter. Recent work by Young et al. (1998) has led to the detection of broad Hα in both total and polarized flux, consistent with our discovery of significant nuclear emission at *R*. In the radio 3C 234 is a classical double FRII source (Leahy, Pooley & Riley 1986).

2141+279 (3C 436, 4C +27.47, B2 2141+27B, NRAO 0665, CTD 132, DA 559, CTA 096)

[$z = 0.215$, $\log_{10}(L_{5\,\mathrm{GHz}}/\mathrm{W\,Hz^{-1}\,sr^{-1}}) = 25.17$]

A large elliptical host galaxy ($r_{1/2} = 21$ kpc) is strongly favoured for this object, with the variable-beta model again yielding an almost perfect de Vaucouleurs law ($\beta = 0.246$), with an insignificant central point source contribution (see Figs A4 and 1d). As can be seen in panel D of Fig. A4, a secondary nucleus lies approximately 0.6 arcsec from the centre of the host galaxy, and

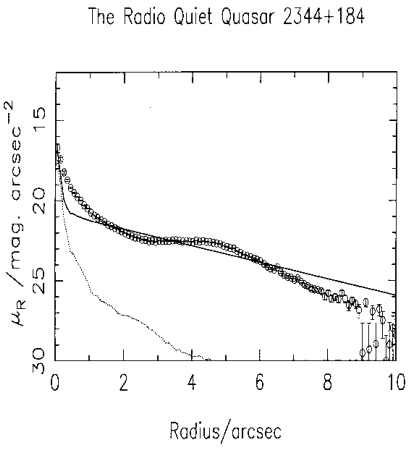

Figure 1 – *continued*

Table 3. The outcome of the variable-β modelling. Column 2 lists the host morphology of the best-fitting 'fixed β' model (results of which are given in Table 2). The best-fitting values for the β profile parameter are given in column 3. The $\Delta\chi^2$ of column 4 quantifies the improvement in fit between this variable-β model and the best-fitting disc or elliptical model. As with Table 2, columns 5 and 6 give the integrated apparent magnitudes of the host galaxy and nuclear component converted to the Cousins R filter. Column 7 lists the ratios of nuclear and integrated host luminosity.

Source	Host	β	$\Delta\chi^2$	$R_{\rm host}$	$R_{\rm nuc}$	$L_{\rm nuc}/L_{\rm host}$
RG						
0345+337	Elliptical	0.249	1.8	18.0	21.1	0.06
0917+459	Elliptical	0.229	263.6	16.0	19.4	0.04
0958+291	Elliptical	0.253	16.0	17.1	18.5	0.27
2141+279	Elliptical	0.246	2.2	16.7	26.1	0.0002
RLQ						
0137+012	Elliptical	0.185	126.3	17.0	17.4	0.72
0736+017	Elliptical	0.193	238.6	16.8	16.2	1.64
1004+130	Elliptical	0.253	4.7	16.9	15.0	5.83
2141+175	Elliptical	0.280	23.0	17.3	16.0	3.44
2247+140	Elliptical	0.249	16.6	17.2	16.9	1.31
2349−014	Elliptical	0.258	9.6	16.0	16.0	0.93
RQQ						
0054+144	Elliptical	0.251	2.9	16.6	15.5	2.75
0157+001	Elliptical	0.238	133.2	15.8	16.2	0.68
0244+194	Elliptical	0.220	47.4	17.5	16.8	1.80
0257+024	Disc	0.754	2850.7	15.9	19.5	0.04
0923+201	Elliptical	0.299	44.0	17.3	15.7	4.60
0953+415	Elliptical	0.266	8.8	18.2	15.2	15.8
1012+008	Elliptical	0.377	101.6	16.8	16.2	1.81
1635+119	Elliptical	0.183	549.6	16.7	18.3	0.23
2344+184	Disc	0.428	1043.8	17.0	19.2	0.12

this can be clearly seen in the model-subtracted image, along with some asymmetrical residual flux and several faint companion objects. The radio source has an FRII morphology (McCarthy, van Breugel & Kapahi 1991).

4.3.2 *The radio-loud quasars*

0137+012 (PKS 0137+012, PHL 1093, 4C 01.04, OC 062, UM 355)

Radio-loud; $[z = 0.258,\ \log_{10}(L_{5\,\rm GHz}/{\rm W\,Hz^{-1}\,sr^{-1}}) = 25.26]$

The modelling results for this object show the host galaxy to be a large elliptical ($r_{1/2}$=13 kpc) which contributes over half of the integrated flux at R (Fig. 1e). The variable-beta model fit is close to elliptical ($\beta = 0.185$), but it does provide a significantly better fit than a pure de Vaucouleurs law. The contour plot in Fig. A5 clearly shows a close companion object (separation ≈1.0 arcsec), which was not resolved in our K-band image. This object was masked out during the model fitting and can clearly be seen in the subtracted image. 0137+012 was one of four objects imaged with the PC camera on *HST* by Disney et al. (1995) using the F702W filter. Using a two-dimensional cross-correlation modelling technique, they also found the host to be a large early-type galaxy. The slightly larger scalelength ($r_{1/2} \simeq 22$ kpc)[1] and fainter host magnitude obtained by their modelling technique is most likely to be due to their use of a synthetic PSF. For a more detailed discussion of the problems associated with two-dimensional modelling and the WFPC PSF see McLure et al. (1999). In the radio the quasar is an FRII source of diameter 42 arcsec with a strong core (Gower & Hutchings 1984a).

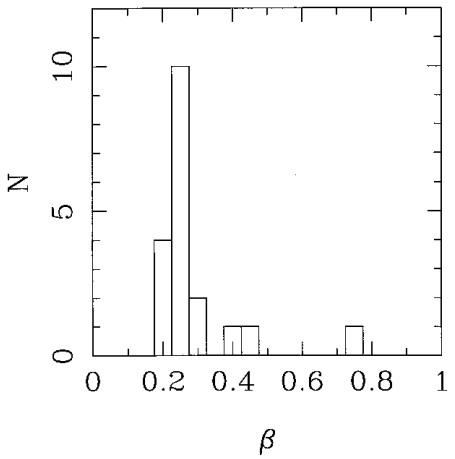

Figure 2. The distribution of β values which results from fitting luminosity profiles of the form $\exp(-r^{\beta})$ to the host galaxies and allowing β to vary as a free parameter in the model fitting. As can be seen from the histogram, 16 of the 19 AGN have host galaxies which follow near-perfect de Vaucouleurs profiles (McLure et al. 1999).

0736+017 (PKS 0736+01, OI 061)

Radio-loud; $[z = 0.191,\ \log_{10}(L_{5\,\rm GHz}/{\rm W\,Hz^{-1}\,sr^{-1}}) = 25.35]$

An elliptical host galaxy is again strongly preferred for this quasar, with a disc host formally excluded (Figs. A6 and 1f). As with 0137+012, the variable-beta modelling confirms the generally spheroidal nature of the host ($\beta = 0.1933$), but it does provide a statistically significant improvement over the pure de Vaucouleurs model. The companion object seen to the south of the quasar, first detected in our K-band image (Dunlop et al. 1993), is not obvious in our new *HST* image shown in Fig. A6. The large area of low-surface-brightness nebulosity to the NE of the quasar which was present in our K-band image is also missing from this R-band image, casting doubt on its reality. At radio wavelengths this quasar is a compact (0.013 arcsec) flat-spectrum source (Gower & Hutchings 1984b; Romney et al. 1984).

1004+130 (PKS 1004+13, PG 1004+130, 4C 13.41, OL 107.7)

Radio-loud; $[z = 0.240,\ \log_{10}(L_{5\,\rm GHz}/{\rm W\,Hz^{-1}\,sr^{-1}}) = 24.94]$

[1] Converted to our cosmology.

As can be seen from the contour plot in Fig. A7 this quasar is a highly nuclear-dominated object in the *R* band. The preferred host galaxy is again an elliptical, although due to the high $L_{\rm nuc}/L_{\rm host}$ ratio the preference is less clear-cut than for most of the other objects. The best-fitting host is fairly large ($r_{1/2} = 8$ kpc) and luminous, although the unresolved nuclear component contributes ≈85 per cent of the integrated flux (Fig. 1g). The results of the variable-beta modelling strongly support the choice of an early-type host ($\beta = 0.253$). 1004+130 is one of the quasars which has also been imaged at the *HST* in the *V* band by Bahcall et al. (1997). They also find the host to be best described by an early-type galaxy, although with a somewhat smaller scale length ($r_{1/2} = 5.8$ kpc). They suggest that there is some sort of structure close into the quasar nucleus. This is beautifully illustrated by our model-subtracted image; two spiral-arm-type features can be clearly seen on either side of the quasar nucleus. The subtracted image also reveals one companion object to the NE, together with two fainter companions to the east. In the radio this quasar is an FRII source of diameter 9 arcmin with a weak core (Miley & Hartsuijker 1978).

2141+175 (OX 169, MC3)

Radio-loud; $[z = 0.213,\ \log_{10}(L_{5\,\rm GHz}/{\rm W\,Hz^{-1}\,sr^{-1}}) = 24.81]$

Our *R*-band image of this complex object shown in Fig. A8 reveals the two extended filaments to the SE and NW previously detected by Smith et al. (1986) and Heckman et al. (1986). The best-fitting host galaxy is a moderate-sized elliptical with $r_{1/2} = 4$ kpc (Fig. 1h), with the variable-beta modelling producing a very similar fit. This quasar has been previously imaged with the *HST* with the F702W filter by Hutchings et al. (1994), who also concluded in favour of an $r^{1/4}$ law but fail to provide any quantitative information on the scalelength of the host galaxy. The model-subtracted image shows the NW filament to be more extended than previously thought, stretching to more than half the length of the SE filament. The hypothesis that the two extensions are composed of old stars (Stockton & Farnham 1991) is supported by their prominence in our existing *K*-band image (Dunlop et al. 1993), and in this emission-line free *HST* image. Also revealed by subtraction of the best-fitting model is a previously undetected companion ≈3 arcsec to the NE of the quasar. In the radio, 2141+175 is a compact (<4 arcsec) flat-spectrum source (Feigelson, Isobe & Kembhavi 1984).

2247+140 (PKS 2247+14, 4C 14.82, OY 181)

Radio-loud; $[z = 0.237,\ \log_{10}(L_{5\,\rm GHz}/{\rm W\,Hz^{-1}\,sr^{-1}}) = 25.31]$

This radio-loud quasar can be seen to be elongated in the NW/SE direction in Fig. A9, as previously reported by Hutchings et al. (1988) and Dunlop et al. (1993). The host galaxy is unambiguously elliptical, with a best-fitting scale length of 11 kpc (Fig. 1i). This preference is again impressively confirmed by the best-fitting beta value of $\beta = 0.249$. The subtracted image reveals two new companion objects embedded in the residual flux of the SE elongation. The quasar is a compact steep-spectrum radio source (van Breugel, Miley & Heckman 1984).

2349-014 (PG 2349-014, PKS 2349-01, PB 5564)

Radio-loud; $[z = 0.173,\ \log_{10}(L_{5\,\rm GHz}/{\rm W\,Hz^{-1}\,sr^{-1}}) = 24.86]$

The *R*-band image of this quasar presented in Fig. A10, shows it to be undergoing an extensive interaction. 2349-014 is included in the sample of Bahcall et al. (1997) (see also Bahcall et al. 1995a), and we confirm their detection of a compact close companion at ≈2 arcsec separation to the east. Bahcall et al. claim that there is no clear evidence for a normal host galaxy centred on the quasar, although they comment that the mean radial profile is well matched by a de Vaucouleurs law. The results of our two-dimensional modelling do not support this. Model-fitting after masking of the most prominent areas of asymmetric nebulosity produces a good match with a large elliptical host galaxy of scalelength $r_{1/2} = 18$ kpc (Fig. 1j). The variable-beta parameter modelling produces a near identical fit ($\beta = 0.258$). The subtracted image highlights the massive tidal arm feature to the north of the quasar and extensive nebulosity to the west. The source of this interaction would appear to be the nearby compact companion. In agreement with Bahcall et al., our new *R*-band data provides little evidence for interaction with the large galaxy to the SE. In the radio this quasar is an FRII source of diameter 53 arcsec with a strong core (Antonucci 1985).

4.3.3 *The radio-quiet quasars*

0054+144 (PHL 909)

Radio-quiet; $[z = 0.171,\ \log_{10}(L_{5\,\rm GHz}/{\rm W\,Hz^{-1}\,sr^{-1}}) = 21.87]$

The host galaxy of this radio-quiet quasar (Fig. A11) is extremely well described by an elliptical template with $r_{1/2} = 8$ kpc, and a disc host is formally excluded (Fig. 1k). The variable-beta modelling again strongly supports this unambiguous choice, settling on a value of $\beta = 0.251$. This object was also imaged with the *HST* at *V* by Bahcall et al. (see Bahcall et al. 1996), and in this case they also found the best-fitting host to be an early-type galaxy. In their *V*-band image Bahcall et al. claim not to detect the extended emission towards the western companion galaxy (off this frame) which was reported in Dunlop et al. (1993). However, the model-subtracted image presented here clearly shows considerable residual luminosity in the direction of the western companion, in agreement with the *K*-band data.

0157+001 (PG 0157+001, Mkn 1014)

Radio-quiet; $[z = 0.163,\ \log_{10}(L_{5\,\rm GHz}/{\rm W\,Hz^{-1}\,sr^{-1}}) = 22.87]$

This spectacular object can clearly be seen to be undergoing massive tidal disruption (Fig. A12). The bright companion object detected at the end of the NE tidal arm in our previous *K*-band image is again detected here, but lies just off the edge of the frame shown in Fig. A12. Also detected in the *R*-band is a faint counter arm to the west, embedded within which are two further bright companion objects. The underlying host galaxy is best described by a bright elliptical galaxy $r_{1/2} = 8$ kpc (Fig. 1l), with the variable-beta modelling choosing a near-perfect elliptical host ($\beta = 0.238$). The full extent of the tidal disruption is revealed by the model-subtracted image. This is the most radio-luminous of the 'radio-quiet' quasars in our sample, and its radio morphology is similar to that found in several radio-loud quasars with an unresolved core accompanied by a secondary component ≈2 arcsec west of the nucleus (Miller, Rawlings & Saunders 1993; Kukula et al. 1998).

0244+194 (1E 0244+1928)

Radio-quiet; $[z = 0.176,\ \log_{10}(L_{5\,\rm GHz}/{\rm W\,Hz^{-1}\,sr^{-1}}) < 21.43]$

The host of this radio-quiet quasar is well described by an large

elliptical galaxy with $r_{1/2} = 9$ kpc (Fig. A13). The variable-beta modelling provides a slightly improved fit with a value of $\beta = 0.220$. The model-subtracted image, shown in Fig. A13, is very clean and shows no obvious signs of any interaction.

0257+024 (US 3498)

Radio-quiet; $[z = 0.115,\ \log_{10}(L_{5\,\mathrm{GHz}}/\mathrm{W\,Hz^{-1}\,sr^{-1}}) = 22.19]$

The host of this radio-quiet quasar is dominated by a disc component with a best-fitting scalelength of $r_{1/2} = 10$ kpc (Fig. 1n). The model-subtracted image in Fig. A14 shows a ring of emission at ≈4 arcsec radius. Also revealed is substantial residual flux in the inner ≈2 arcsec where the host galaxy is bulge-dominated. This feature can also be clearly seen in the luminosity profile shown in Fig. 1(n). As a result of the central bulge, the variable-beta model chooses a substantially lower value of beta (0.75), and offers a significantly better χ^2 fit than a pure exponential disc. Nevertheless, this transpires to be the most disc-dominated host galaxy in the quasar sample observed to date.

0923+201 (PG 0923+201, Ton 1057)

Radio-quiet; $[z = 0.190,\ \log_{10}(L_{5\,\mathrm{GHz}}/\mathrm{W\,Hz^{-1}\,sr^{-1}}) < 21.66]$

This radio-quiet quasar is a member of a small group of galaxies. The two large galaxies in Fig. A15 to the SE and SW are at the same redshift as the quasar (Heckman et al. 1984), and 0923+201 was thought to be possibly interacting with these (Hutchings, Janson & Neff 1989). However, our two-dimensional modelling provides little evidence for any obvious interaction. The host is extremely well matched by a standard elliptical template (Fig. 1o), with the variable-beta model also choosing an approximately de Vaucouleurs model ($\beta = 0.3$). The subtracted image is very clean and symmetrical, but with perhaps a suggestion of more residual flux in the direction of the SE companion.

0953+415 (K438−7, PG 0923+415)

Radio-quiet; $[z = 0.239,\ \log_{10}(L_{5\,\mathrm{GHz}}/\mathrm{W\,Hz^{-1}\,sr^{-1}}) < 21.69]$

This radio-quiet quasar is the most heavily nuclear-dominated object in the sample. This can be seen immediately by its stellar-like appearance in the grey-scale of Fig. A16. The best-fitting host is a medium-sized elliptical of scalelength $r_{1/2} = 7$ kpc (Fig. 1p). However, due to the faintness of the host relative to the unresolved nuclear component, we are unable to exclude a disc host with a high level of confidence. Despite this, we are still able to constrain the relative luminosity of the AGN and host components, since both the alternative host models yield similar values. 0953+415 is another object which was imaged with the *HST* in *V* by Bahcall et al. (1994, 1997). From their *V*-band image Bahcall et al. were unable to clearly detect a bright host galaxy centred on the quasar. It seems likely that this inconsistency arises primarily from the procedure used by Bahcall et al. to subtract the PSF. As can be seen from the luminosity profile shown in Fig. 1(p), the unresolved AGN component dominates to a radius of only ≈2 arcsec. Normalization of the PSF in a annulus between 1 and 3 arcsec (as performed by Bahcall et al. 1997) will therefore lead to a substantial over-subtraction. Tests on our own data show that this effect is more than sufficient to explain the non-detection by Bahcall et al. The model-subtracted image reveals a tidal arm feature to the SW, along with up to four possible companion objects.

1012+008 (PG 1012+008)

Radio-quiet; $[z = 0.185,\ \log_{10}(L_{5\,\mathrm{GHz}}/\mathrm{W\,Hz^{-1}\,sr^{-1}}) = 22.00]$

This radio-quiet quasar is another dramatically interacting object which was also imaged in the *V*-band byBahcall et al. (1997). In the grey-scale of Fig. A17 the quasar is seen together with two companion galaxies to the north and east. The best-fitting host is a large elliptical with $r_{1/2} = 23$ kpc (Fig. 1q), a result supported by the variable-beta modelling result ($\beta = 0.377$). We note that, using two-dimensional modelling, Bahcall et al. (1997) concluded that the host was a disc galaxy with $r_{1/2} = 10.8$ kpc (after conversion to our adopted cosmology); however, Bahcall et al.'s best fit to the one-dimensional profile of this galaxy is an elliptical with $r_{1/2} = 24.5$ kpc, in excellent agreement with our result (this perhaps indicates that there is a problem with the method of two-dimensional modelling implemented by Bahcall et al.). From the model-subtracted image shown in panel D it is clear that the eastern companion is definitely interacting, with the northern companion perhaps also involved.

1635+119 (MC 2)

Radio-quiet; $[z = 0.146,\ \log_{10}(L_{5\,\mathrm{GHz}}/\mathrm{W\,Hz^{-1}\,sr^{-1}}) = 23.02]$

The host of this radio-quiet quasar is best-matched by a moderate-sized elliptical ($r_{1/2} = 6$ kpc) with a disc host being formally excluded (Fig. 1r). The model-subtracted image in Fig. A18 shows residual luminosity around the core of the quasar, unaccounted for by the standard elliptical template. This is confirmed by the variable-beta modelling, which shows a statistically significant improvement in the quality of fit with a beta parameter of $\beta = 0.184$. The model-subtracted image also shows numerous companion objects in this field.

2344+184

Radio-quiet; $[z = 0.138,\ \log_{10}(L_{5\,\mathrm{GHz}}/\mathrm{W\,Hz^{-1}\,sr^{-1}}) < 21.18]$

The modelling of this object presented here must still be regarded as preliminary. The raw *R*-band image presented in Fig. A19 shows this quasar to be residing in a disc galaxy with clearly evident spiral arms. A two-dimensional disc template of scalelength $r_{1/2} = 9$ kpc can reasonably reproduce the total luminosity of the object, but is obviously unable to cope with the spiral arms. As can clearly be seen from both the luminosity profile (Fig. 1s) and model-subtracted image, the inner ≈2 arcsec are dominated by a bulge with a different position angle from the main disc. A two-component model must therefore be adopted in order to properly analyse this quasar host.

5 DISCUSSION

A complete discussion of our results is not appropriate until all the sources in our matched samples have been observed. However, the initial results presented above suggest the emergence of several potentially important trends which deserve comment at this stage. Furthermore, since the majority of RQQs in our sample have in fact been observed, this interesting subsample of objects is already approaching completion, and we can draw some fairly robust conclusions regarding the nature of the RQQ population.

Table 4. Absolute magnitudes (M_R), and optical–infrared ($R-K$) colours of the best-fitting host galaxy and nuclear component for each AGN. Columns 2 and 3 give the *R*-band absolute magnitudes (M_R) derived from the current modelling of the *HST* data, assuming a spectral index of $\alpha = 1.5$ (where $f_\nu \propto \nu^{-\alpha}$) for the galaxy and $\alpha = 0.2$ for the quasar. Columns 4 and 5 list the $R-K$ colours of the host galaxy and nuclear component respectively. These colours were derived by combining 12-arcsec aperture *R*-band photometry from our *HST*-based models with the 12-arcsec aperture *K*-band photometry derived by Taylor et al. (1996), to minimize the uncertainty introduced by errors in constraining the galaxy scalelengths at *K*.

Source	M_R(host)	M_R(nuc)	$(R-K)_{\rm host}$	$(R-K)_{\rm nuc}$
RG				
0345+337	−23.05	−19.63	3.23	5.32
0917+459	−24.20	−20.65	2.83	4.49
0958+291	−23.25	−21.70	3.03	3.97
2141+279	−24.09	−14.94	3.02	9.85
RLQ				
0137+012	−24.04	−23.53	2.81	3.15
0736+017	−23.58	−24.01	3.15	2.73
1004+130	−24.10	−25.70	2.96	2.22
2141+175	−23.51	−24.52	2.53	1.97
2247+140	−23.80	−23.80	2.81	2.60
2349−014	−24.32	−24.00	2.86	3.64
RQQ				
0054+144	−23.62	−24.49	3.14	1.32
0157+001	−24.29	−23.70	2.94	2.82
0244+194	−22.77	−23.24	2.54	2.72
0257+024	−23.32	−19.69	2.70	4.66
0923+201	−23.25	−24.57	3.36	2.66
0953+415	−22.82	−25.52	2.84	2.59
1012+008	−23.78	−23.95	3.78	1.72
1635+119	−23.05	−21.54	3.27	3.23
2344+184	−22.54	−20.30	3.11	4.66

5.1 Host-galaxy luminosities and morphologies

The most striking initial result of this study is that our observing strategy, combined with modelling incorporating a high-dynamic-range PSF, has enabled us not only to detect easily all of the host galaxies observed to date, but also to determine unambiguously the morphological type of the host in virtually every case (see Tables 2 and 3, and Figs 1 and 2). This represents a major improvement on previous *HST*-based quasar-host studies, which in some cases have actually struggled to detect any host galaxy emission (Bahcall et al. 1994, 1997), leading the authors to conclude that some quasars lie in low-luminosity host galaxies. Our results to date (which include imaging of several of the quasars also imaged by Bahcall et al.) indicate that such conclusions were erroneous. In contrast, as detailed in Table 4 and illustrated in Fig. 3, we confirm the basic result of our ground-based *K*-band study that *all* the quasars in our sample lie in host galaxies with luminosities $\geq 2L^*$ (see the notes on 0953+415 in Section 3 for a detailed discussion of the most likely explanation for Bahcall et al.'s struggle to detect this host galaxy). A similar result with regard to host luminosities has recently been reported from the *HST* imaging of LBQS quasars at $z > 0.4$ by Hooper, Impey & Foltz (1997) (although in this work no attempt was made to identify the morphological type of the hosts of these slightly higher redshift quasars).

As hoped, these *HST* images have enabled us to improve substantially on our *K*-band study in terms of discerning the morphological type of the hosts. All of the radio galaxies and RLQ hosts we have observed to date can be unambiguously classified as massive elliptical galaxies, with scalelengths in the range 6–23 kpc, consistent with unification of RGs and RLQs via orientation effects. Perhaps more unexpectedly, all except the two least-luminous RQQs are also found to lie in massive ellipticals, placing on a firm statistical footing the tentative result reported by Disney et al. (1995) and Taylor et al. (1996) that luminous RQQs lie in massive ellipticals, despite the fact that the less-luminous, radio-quiet Seyfert galaxies are predominantly disc-dominated. Thus, whatever the true physical origin of radio loudness, it is clearly not simply a consequence of the morphological type of the host galaxy. A particularly striking feature of this result is the extent to which a pure $r^{1/4}$ law provides an essentially perfect description (apart from obvious tidal tails and secondary nuclei) of the hosts of 16 out of the 19 AGN observed in our sample to date.

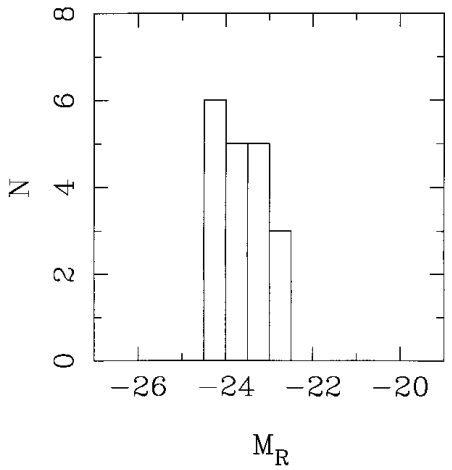

Figure 3. The distribution of (integrated) *R*-band absolute magnitudes (M_R) displayed by the best-fitting host galaxies. The adopted fiducial integrated absolute magnitude M_R^* corresponding to an L^* galaxy is $M_R^* = -22.2$, which is derived from the most recent determination of M_R^* by Lin et al. (1996) ($M_R^* = -21.8$) after correcting to an integrated magnitude. All the host galaxies have $L > 2L^*$.

5.2 Relation to 'normal' massive elliptical galaxies

5.2.1 Scalelengths, the Kormendy relation and axial ratios

The distribution of derived host-galaxy scalelengths is shown in Fig. 4. With the exception of the RLQ 2141+175, for which accurate scalelength determination is problematic due to the complexity of the observed interaction, the half-light scalelengths of all the host galaxies are consistent to within a factor of 3. The homogeneity of these host galaxies is striking when they are plotted on the $\mu_e - r_e$ projection of the fundamental plane (see Fig. 5), where we find that they describe a Kormendy relation essentially identical to that displayed by 'normal' massive ellipticals (Schneider, Gunn & Hoessel 1983; Capaccioli, Caon & D'Onofrio 1992); a least-squares fit yields the relationship $\mu_{1/2} = 3.34_{\pm 0.50} \log_{10} r_{1/2} + 17.95_{\pm 0.53}$. Thus the basic morphological parameters of these host galaxies appear to be indistinguishable from those of normal, inactive massive ellipticals.

If this conclusion is correct, then the host galaxies should also display a distribution in axial ratios which is indistinguishable from that displayed by the normal elliptical galaxy population,

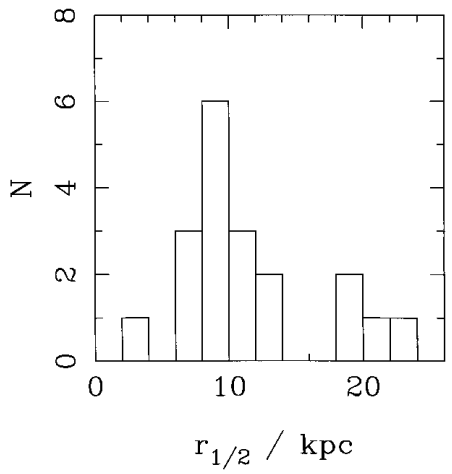

Figure 4. The distribution of scalelengths displayed by the best-fitting host galaxies. All scalelengths are presented as half-light radii ($r_{1/2}$) to facilitate ease of comparison between the sizes of disc and elliptical hosts.

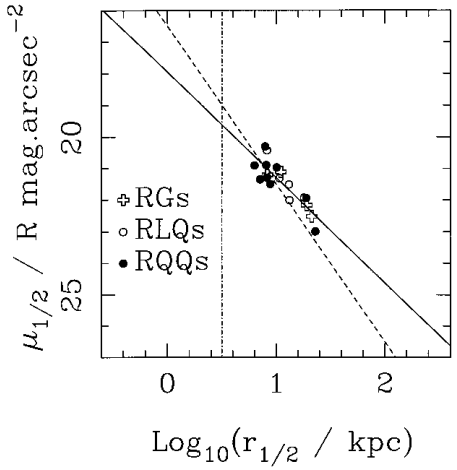

Figure 5. The Kormendy surface brightness/scalelength relation ($\mu_{1/2}$ versus $r_{1/2}$) displayed by the host galaxies of the RGs (crosses), RLQs (open circles) and RQQs (filled circles). Also shown on the plot are the best-fitting relation described in the text (solid line; slope $\simeq 3$), a line indicating the locus of constant galaxy luminosity (dashed line; slope = 5), and the dividing line between normal ellipticals and brightest cluster members as determined by Capaccioli et al. (1992) (dot-dashed line).

which peaks at $b/a > 0.8$ (Sandage, Freeman & Stokes 1970; Ryden 1992). The axial ratios yielded by the model-fitting are given in Table 2, and the resulting host-galaxy axial-ratio distribution is plotted in Fig. 6. It is perfectly consistent with the distribution displayed by normal ellipticals and, with only one object displaying an axial ratio $b/a < 0.6$, is completely at odds with the recent results of Hooper et al. (1997), who reported that *most* of the hosts of bright quasars at $z \simeq 0.4$ have low axial ratios $b/a < 0.6$. However, Hooper et al. expressed the concern that their result might reflect high-surface-brightness features such as bars or tidal tails, rather than the axial ratio of the underlying stellar population, and our very different result, based on proper modelling of the underlying host, indicates that this is almost certainly the correct explanation for their apparently contradictory conclusion.

5.2.2 *Colours*

One of the reasons we elected to use the F675W filter rather than the F606W filter used by Bahcall et al. was the evidence, gleaned from our deep off-nuclear spectroscopy of quasar hosts (Kukula et al. 1997; Hughes et al. 1999), that most quasar hosts appear to be rather red galaxies with a clear 4000-Å break in their spectrum. We are now, for the first time, in a position to check whether this is indeed the case by combining our new *R*-band *HST* results with the *K*-band results of Taylor et al. (1996) to measure the $R-K$ colours of the RGs and quasar hosts. The results are listed in Table 4, and plotted in Fig. 7, where the observed colours are compared with those predicted from simple *k*-correction of stellar populations with ages of 8, 12 and 16 Gyr (Guiderdoni & Rocca-Volmerange 1987). The uncertainty in the $R-K$ colours of the radio galaxies is only $\simeq 0.15$ mag, and it is striking that these four objects track almost perfectly the *k*-correction derived from the

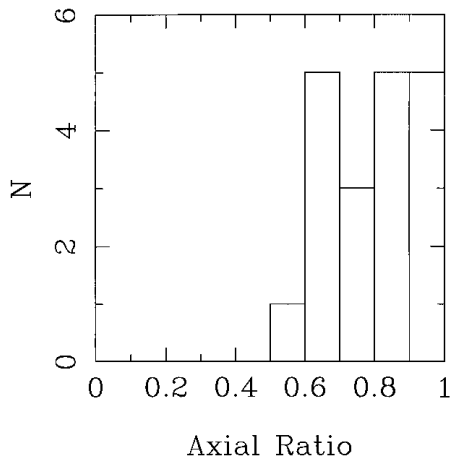

Figure 6. The distribution of axial ratios displayed by the model host galaxies. The distribution is consistent with that displayed by the normal elliptical galaxy population, which peaks at $b/a > 0.8$ (Sandage, Freeman & Stokes 1970; Ryden 1992).

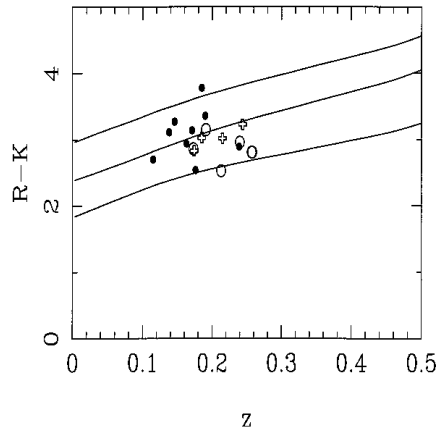

Figure 7. The apparent R–K colours of the hosts (RGs = crosses, RLQs = open circles, RQQs = filled circles) plotted against redshift, compared with the colours predicted from simple *k*-correction of stellar populations with ages of 8, 12 and 16 Gyr (Guiderdoni & Rocca-Volmerange 1987). The uncertainty in the $R-K$ colours of the radio galaxies is only $\simeq 0.15$ mag, and it is striking that these four objects track almost perfectly the *k*-correction derived from the SED of an old (12 Gyr) elliptical galaxy. The uncertainties associated with removal of the nuclear contribution mean that the $R-K$ colours of the quasar hosts are somewhat more uncertain ($\simeq$ 0.3–0.5 mag), but with the present data it is clear that the hosts of all three classes of powerful AGN have colours which are consistent with each other, and with that of mature stellar populations.

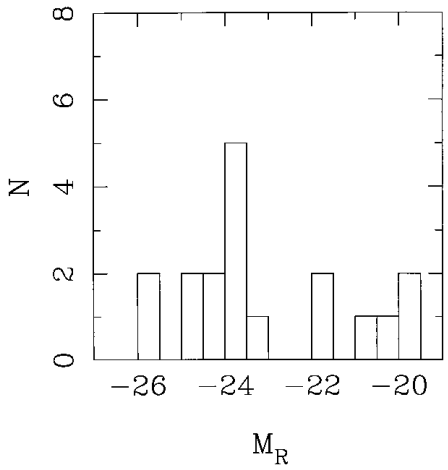

Figure 8. The distribution of R-band absolute magnitudes (M_R) displayed by the best-fitting unresolved nuclear components.

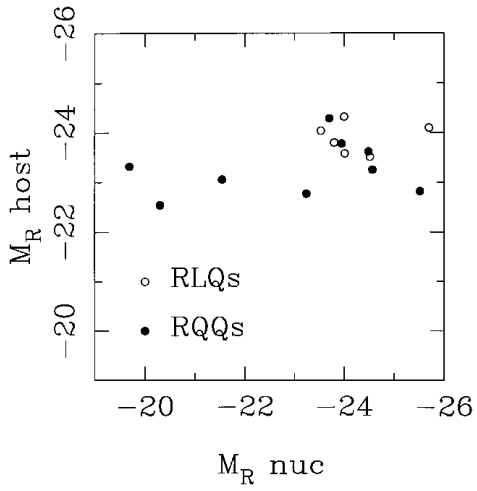

Figure 9. Absolute host galaxy magnitude plotted against absolute nuclear magnitude at R (RLQs = open circles, RQQs = filled circles). The correlation is not statistically significant ($p = 0.376$), but is consistent with the existence of a minimum host-galaxy luminosity for the production of a luminous quasar.

SED of an old (12 Gyr) elliptical galaxy. The uncertainties associated with removal of the nuclear contribution mean that the $R–K$ colours of the quasar hosts are somewhat more uncertain ($\simeq$ 0.3–0.5 mag), but with the present data it is clear that the hosts of all three classes of powerful AGN have colours which are consistent with each other, and with that of old, passively evolving stellar populations. Model-independent support for this conclusion can be gleaned by comparing Fig. 8 with the $R - K$ versus z plot for objects detected in a K-band survey reaching $K \simeq 17.3$ (Glazebrook et al. 1995); the host galaxy $R - K$ colours shown in Fig. 8 track well the red envelope displayed by K-band selected galaxies at comparable redshifts.

This is the first clear evidence that the dominant stellar populations in not only RGs, but also quasar hosts have ages comparable to the oldest known elliptical galaxies, and thus must have formed at high redshift ($z > 4$; Dunlop 1999). It also means that any substantial star formation activity associated with the triggering of AGN activity must either be dust-enshrouded, or confined either to the nuclear regions of the galaxy (in which case it will have been attributed to the quasar nucleus in our modelling procedure) or to obvious tidal tails, which we have excised prior to modelling the host galaxy.

5.2.3 Interactions

Previous *HST* studies have emphasized the variety of environments found around quasars, ranging from highly distorted or obviously interacting systems to apparently isolated, undisturbed galaxies (e.g. Disney et al. 1995; Bahcall et al. 1997). In their sample of 20 quasars with $z < 0.3$, Bahcall et al. found only three host galaxies currently undergoing major interactions (although as many as 13/20 quasar hosts had close companions with at least the possibility of gravitational interaction).

At first sight our own images appear to tell a similar story, with a relatively low occurrence of obvious, large-scale disturbance. However, as can be seen from panel D in Figs 1(a)–(s), removal of the axisymmetric model for the underlying host galaxy makes it relatively easy to identify morphological peculiarities such as excess flux, tidal tails, close companions and secondary nuclei, all of which have been linked to galaxy interactions, often at considerably lower surface brightness levels than the more obvious morphological distortions masked out prior to host-galaxy modelling. A full statistical analysis of the prevalence and strength of such features is deferred until completion of the sample, but here we simply note that, despite our basic conclusion that the host galaxies are relatively passive massive ellipticals, three out of the four RGs, five out of the six RLQs and six out of the nine RQQs observed to date show one or other of the morphological peculiarities mentioned above.

This tally serves to emphasize that most of these AGN may have been triggered into action by the interaction of their (perhaps previously completely passive) host galaxy with a companion object. However, we add the cautionary note that the true significance of such apparently impressive interaction statistics (14 out of 19 AGN) can only really be judged against the results of a comparably detailed investigation of the morphologies of ‘inactive’ massive ellipticals. This issue will be covered in more detail by Dunlop et al. (in preparation).

5.3 The AGN–host connection

The absolute magnitudes (M_R) of the fitted nuclear components are given in Table 4, and the resulting distribution is presented in Fig. 8. The nuclear absolute magnitudes are then plotted against the host absolute magnitudes in Fig. 9. Only a weak correlation ($p = 0.376$, using the Spearman rank correlation test) is seen, consistent with our previous finding at K. However, the fact that the hosts of the two faintest quasars in our sample contain a significant disc component suggests that a more significant correlation might be revealed if only bulge luminosity is considered for comparison with nuclear power. This possibility is explored below in the context of recent studies of nearby galaxies which suggest that black hole mass does indeed depend primarily on bulge mass rather than total galaxy mass.

5.3.1 The black hole–spheroid connection

Our unambiguous finding that all the quasars in our sample with $M_R < -23.5$ lie in massive elliptical galaxies, irrespective of radio power, clearly refutes the long-standing hypothesis that, like the majority of Seyferts, radio-quiet quasars lie in predominantly disc

Table 5. The results of calculating spheroid mass, and hence black hole mass/luminosity from host-galaxy spheroid luminosity. Column 2 gives the derived spheroid mass (in units of $10^{11}\,M_{\odot}$), calculated from the values of M_R given in Table 4 using the mass:light ratio relation given by Magorrian et al. (1998). Column 3 then gives the estimated mass of the central black hole (in units of $10^{9}\,M_{\odot}$) derived from the data in column 2 using the high-mass form of the $m_{\rm sph} : m_{\rm bh}$ relation deduced by Magorrian et al. (1998), while columns 4 and 5 give alternative estimates of $m_{\rm bh}$ based on $P^{\rm total}_{\rm 5-GHz}$ and $P^{\rm core}_{\rm 5-GHz}$ Finally column 6 gives the predicted Eddington M_R corresponding to $m^{a}_{\rm bh}$ given in column 3.

Source	$m_{\rm sph}/10^{11}\,M_{\odot}$	$m^{a}_{\rm bh}/10^{9}\,M_{\odot}$	$m^{b}_{\rm bh}/10^{9}\,M_{\odot}$	$m^{c}_{\rm bh}/10^{9}\,M_{\odot}$	M_R(Eddington)
RG					
0345+337	6.3	5.0	20		−24.8
0917+459	22	33	25	25	−28.3
0958+291	7.8	6.9	17	34	−25.4
2141+279	20	27	16	19	−27.9
RLQ					
0137+012	18	25	17	58	−27.8
0736+017	11	12	22		−26.4
1004+130	20	28	13	15	−28.0
2141+175	10	11	12		−26.2
2247+140	14	17	18		−27.1
2349−014	25	40	12	45	−28.6
RQQ					
0054+144	12	13	0.9	3.7	−26.5
0157+001	24	38	2.2	11	−28.5
0244+194	4.6	3.2	<0.6	<2.3	−24.0
0257+024	3.2	1.8	1.2	4.2	−22.9
0923+201	7.8	6.9	<0.8	<3.0	−25.4
0953+415	4.9	3.4	<0.8	<3.1	−24.1
1012+008	14	16	1.0	4.2	−26.2
1635+119	6.3	5.0	2.5	12	−24.8
2344+184	2.9	1.6	<0.5	<1.8	−22.6

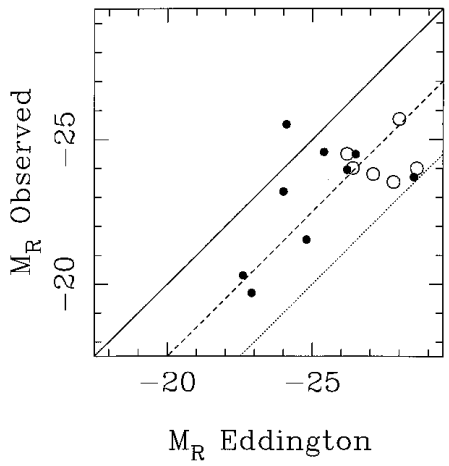

Figure 10. The observed absolute magnitude M_R of the nuclear component in each quasar plotted against the absolute magnitude, which is predicted by assuming that each quasar contains a black hole of mass $m_{\rm bh} = 0.006 m_{\rm spheroid}$, and that the black hole is emitting at the Eddington luminosity(RLQs = open circles, RQQs = filled circles). The black hole mass has been calculated from the host galaxy bulge luminosity, assuming the mass to light ratio and $m_{\rm spheroid} - m_{\rm BH}$ correlation given in Magorrian et al. (1998). The solid line shows where the quasars should lie if they were all radiating at their respective Eddington luminosities, while the dashed line indicates 10 per cent of predicted Eddingtion luminosity, and the dotted line indicates 1 per cent of predicted Eddington luminosity. As in previous figures, the RLQs are indicated by open circles, while the RQQs are indicated by filled circles. The nuclear components of the radio galaxies are not plotted, because all the evidence suggests they are substantially obscured by dust.

galaxies. However, if it is accepted that all quasars (radio-loud and radio-quiet) result from accretion of material on to a supermassive black hole, then our result can be seen as a natural consequence of the black hole/spheroid mass correlation recently derived for nearby galaxies by Magorrian et al. (1998), as we now briefly explain.

Magorrian et al. find that the available kinematic data on nearby galaxies are consistent with the relation $m_{\rm bh} = 0.006 m_{\rm sph}$ where $m_{\rm sph}$ is the mass of the hot stellar component (i.e., the spheroidal bulge), strengthening the previous conclusion of Kormendy & Richstone (1995). They also show that $m_{\rm sph}$ can be estimated from the luminosity of the spheroidal component using a mass:light ratio which is proportional to $M^{0.18}$ (their equation 10), broadly consistent with the fundamental-plane correlation predicted using the virial theorem (e.g. Bender, Burstein & Faber 1992).

Since we now possess the first reliable determinations of the spheroid luminosity for the hosts of a significant sample of AGN, we have explored the result of applying these two relations to estimate (albeit rather crudely) the spheroidal mass $M_{\rm sph}$ of each host, and hence the *expected* mass of the black hole at the centre of each galaxy. The results of this calculation are listed in Table 5, columns 2 and 3. We have then proceeded to calculate the Eddington luminosity, Eddington temperature, and hence Eddington absolute magnitude M_R for the putative black hole at the centre of each host galaxy, and the results of this calculation are given in column 6 of Table 5, and compared with the observed nuclear absolute magnitude of each quasar (i.e., after host galaxy removal) in Fig. 10.

In our view, this is a surprisingly successful calculation. As can be seen from Fig. 10, the maximum luminosity produced by any quasar is comparable with the predicted Eddington limit, while the

majority appear to be radiating at a few per cent of the Eddington luminosity. Moreover, despite the large number of sources of potential scatter, the correlation between observed M_R and predicted Eddington M_R is stronger ($p = 0.164$) than that between raw host-galaxy luminosity and nuclear lumonsity [and becomes significant ($p = 0.07$) if 0953+415 is excluded from the analysis], and both the radio-quiet and radio-loud quasars display a similar relation. This suggests that, in both classes of quasar, the *optical* luminosity arises from a similar process of accretion on to a massive black hole, and that RLQs and RQQs of comparable absolute magntiude $M_R < -23.5$ are powered by black holes of comparable mass $M > 3 \times 10^9\,\mathrm{M}_\odot$.

The results of this calculation can be regarded as providing independent evidence that the relation of Magorrian et al. still applies for large galaxy and black hole masses. To reiterate, this relation would predict that such massive black holes can only be housed in galaxies with a spheroid mass of $> 5 \times 10^{11}\,\mathrm{M}_\odot$ which is equivalent to an absolute magnitude of $M_R < -23$, which is exactly what we find. Galaxies with such massive spheroidal components must inevitably be classed as giant ellipticals, in which case it could be regarded as a (now successful) prediction of the black hole/spheroid mass relation that all luminous quasars must reside in massive elliptical galaxies more luminous than $\simeq 2L^*$.

5.3.2 *The black hole–radio power connection*

Finally, we combine our estimates of black hole mass derived from host-galaxy spheroid mass (Table 5) with the radio data available to us for each object to investigate how our results compare with the radio luminosity–black hole mass correlations recently derived for low-redshift galaxies by Franceschini, Vercellone & Fabian (1998).

Franceschini et al. found a remarkably tight relationship between black hole mass and both total and nuclear radio centimetric luminosity, with a very steep dependence of the radio power on the mass of the black hole $m_{\rm bh}$ ($P^{\rm tot}_{5\,\rm GHz} \propto m_{\rm bh}^{2.7}$). In Fig. 11(a) we have replotted their data which demonstrate the relation between total 5-GHz radio luminosity and black hole mass in nearby galaxies, along with their best-fitting straight-line relation, highlighting the location of the Milky Way and M87. We have then added the relevant datapoints (or upper limits) for the AGN studied in this paper. Whereas Franceschini et al. were able to determine $m_{\rm bh}$ directly from high-resolution spectroscopy, the value of $m_{\rm bh}$ plotted for each of our AGN has of course had to be inferred from the mass of the spheroidal component of its host galaxy. However, the location of our AGN on this diagram, particularly the radio-loud AGN, strongly suggests that our host-galaxy-based black hole mass estimates are reasonable, despite the large uncertainties involved in extrapolating from spheroid luminosity.

To put this another way, one can derive two completely independent estimates of the mass of the black hole at the heart of each of our AGN using either (i) the luminosity of the host spheroid and the relations given by Magorrian et al. as described above, or (ii) the $P_{5\,\rm GHz} : m_{\rm bh>}$ regression line of Franceschini et al. shown in Fig. 11(a), and for the radio-loud AGN in our sample these values agree to within a factor of typically 2 (rms – see columns 3 and 4 of Table 5).

Since the RGs and RLQs appear so consistent with the $P_{5\,\rm GHz} : m_{\rm bh}$ relation, it is inevitable that the RQQs should lie below it, but a striking feature of Fig. 11(a) is that (albeit that a number of upper limits are involved), there does still appear to be a correlation between radio luminosity and host-galaxy-derived $m_{\rm bh}$ within the RQQ subsample. This suggests that the radio luminosities of the RQQs might also be linked to those of lower

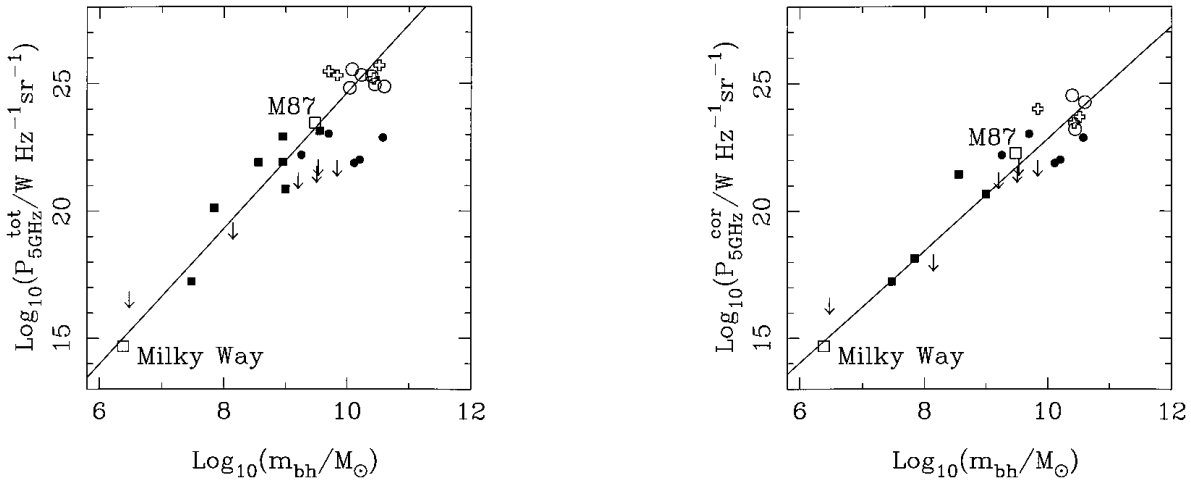

Figure 11. (a) Total radio luminosity $P^{\rm total>}_{5\,\rm GHz}$ versus black hole mass showing the data on low-redshift 'normal' galaxies from Franceschini, et al. (1998), and the AGN discussed in this paper (RGs = crosses, RLQs = open circles, RQQs = filled circles). The solid line is simply the best-fitting relation to the nearby galaxy data given by Franceschini et al. – $\log(P^{\rm total}_{5\,\rm GHz}) = 2.73\log(m_{\rm bh}) - 2.87$. For the nearby galaxies $m_{\rm bh}$ has been estimated directly from stellar dynamics, while for the AGN $m_{\rm bh}$ has been estimated from host-galaxy spheroid luminosity using the relations derived by Magorrian et al. (1998). (b) Core radio luminosity $P^{\rm core}_{5\,\rm GHz}$ versus black hole mass showing the data on low-redshift 'normal' galaxies from Franceschini et al. (1998), and the AGN discussed in this paper (RGs = crosses, RLQs = open circles, RQQs = filled circles) for which a core radio flux was available in the literature, with little evidence for a signficant beamed component. The solid line is the relation $P \propto m_{\rm bh}^{2.2}$ expected for simple advection-dominated accretion models (Fabian & Rees (1995), or indeed for any model in which the emission is mostly dependent of the emitting area available around a black hole) normalized to the Milky Way. Unlike Franceschini et al., we have attributed all the radio emission from M31 (after removal of very extended radio emission linked to star formation) to the core, because the AGN contribution in M31 would in fact be remain unresolved at the distance of most of the objects in even the local sample; this appears to the reason that we find the core radio data to be linked to $m_{\rm bh}$ through a flatter relation $P^{\rm core}_{5\,\rm GHz} \propto m_{\rm bh}^{2.2}$ than did Franceschini et al.

mass objects via a simple relation. Since the study of Kukula et al. (1998) has shown that the radio emission from these RQQs, where detectable, arises entirely from a compact core-like component, we have therefore investigated whether the radio properties of RQQs can be linked to those of nearby galaxies if only compact radio emission is included.

This is explored in Fig. 11(b). Franceschini et al. also found a strong correlation between core 5-GHz radio luminosity and black hole mass, and so we have again reproduced their data for nearby galaxies, this time plotting $P^{\rm core}_{\rm 5\,GHz}$ versus $m_{\rm bh}$, along with the relation $P \propto m_{\rm bh}^{2.2}$ expected for simple advection-dominated accretion models (Fabian & Rees 1995), or indeed for any model in which the emission is mostly dependent on the emitting area available around a black hole. We have replotted all the RQQ data points shown in Fig.11(a), but this time have only plotted datapoints for the cores of the lobe-dominated radio-loud AGN (to minimize the impact of beaming; Giovannini et al. 1988; Lister & Gower 1994). We note that in this case the RQQs apparently form a natural extension of the local galaxy sample, as do the least luminous cores of the radio-loud AGN, and that the plotted relation provides an excellent description of the data. A number of points are worthy of comment. First, unlike Franceschini et al. we have attributed all the radio emission from M31 (after removal of very extended radio emission linked to star formation) to the core because the AGN contribution in M31 would in fact remain unresolved at the distance of most of the objects in even the local sample; this appears to be the reason that we find the core radio data to be linked to $m_{\rm bh}$ through a flatter relation $P^{\rm core}_{\rm 5\,GHz} \propto m_{\rm bh}^{2.2}$ than did Franceschini et al.. Second, it is noteworthy that M87 moves from the 'radio-loud' relation in Fig. 11(a), to the 'radio-quiet' relation in Fig. 11(b) once its extended radio emision is removed, as do several of the radio-loud AGN. Third, as is clear from the figure, several of the RQQs currently only possess upper limits on radio luminosity; if $P^{\rm core}_{\rm 5\,GHz}$ and $m_{\rm sph}$ really are both good indicators of the black hole mass in these objects, then we would predict that the radio emission from these RQQs should be detected by radio observations reaching only an order of magnitude below the current limits.

Because it is undoubtedly possible that $P^{\rm core}_{\rm 5\,GHz}$ is a better indicator of black hole mass than is $m_{\rm sph}$, we have used the relation shown in Figure 11(b) to obtain an independent prediction of $m_{\rm bh}$ for each quasar, and the results are presented in column 5 of Table 5. In Fig. 12 we plot $m_{\rm bh}$ derived from $P^{\rm core}_{\rm 5\,GHz}$ against $m_{\rm bh}$ derived from host galaxy luminosity. These *completely independent estimates* of $m_{\rm bh}$ are clearly extremely well correlated ($p = 0.003$), and for individual sources the discrepancy is no greater than a factor of 4, and is frequently smaller. However, use of the $P^{\rm core}_{\rm 5\,GHz} - m_{\rm bh}$ relation shown in Fig. 11(b), does tend to yield smaller black hole masses for the RQQs than the use of $m_{\rm sph}$.

5.4 The origin of radio loudness

Despite the good agreement between the black hole masses of the radio-loud AGN as estimated from $P^{\rm total}_{\rm 5\,GHz}$ and host galaxy luminosity, it seems unlikely that the relation shown in Fig. 11(a) can be a fair indicator of the black hole masses in the RQQs, because then the more luminous RQQs such as 0054+144 would appear to have an optical luminosity an order of magnitude greater than the Eddington luminosity.

This leaves either $P^{\rm core}_{\rm 5\,GHz}$ or host-galaxy luminosity as potential

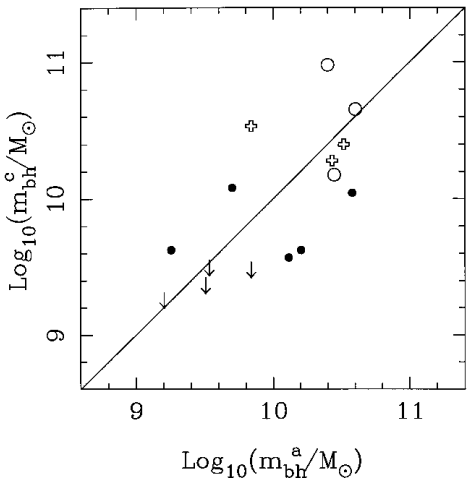

Figure 12. Black hole mass ($m^{\rm c}_{\rm bh}$ – as given in column 5 of Table 5) as estimated from core radio flux $P^{\rm core}_{\rm 5\,GHz}$ plotted against black hole mass ($m^{\rm a}_{\rm bh}$ – as given in column 3 of Table 5) estimated from host galaxy luminosity. These two completely independent estimators of black hole mass are highly correlated ($p = 0.003$), and for individual objects agree to no worse than a factor of 4.

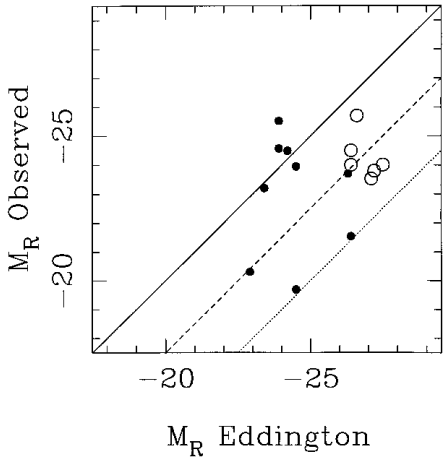

Figure 13. As Fig. 11, but this time with Eddington M_R derived using the values of $m_{\rm bh}$ estimated from $P^{\rm core}_{\rm 5\,GHz}$.

alternative estimators of black hole mass, and while Fig. 12 demonstrates that both quantities lead to reasonably consistent values for $m_{\rm bh}$, the implication for the physical origin of radio loudness depends rather crucially on which of these is the more reliable predictor of $m_{\rm bh}$. The reason for this is that, for the radio-loud objects, comparison of columns 3, 4 and 5 in Table 5 shows that essentially all routes of black hole mass estimation lead to values of $m_{\rm bh} > 10^{10}\,{\rm M}_{\odot}$. However, for the RQQs, use of $P^{\rm core}_{\rm 5\,GHz}$ to estimate $m_{\rm bh}$ produces values typically a factor of 2 smaller than inferred from host-galaxy luminosity, and implies that *no* RQQ in the sample has a black hole more massive than $m_{\rm bh} = 10^{10}\,{\rm M}_{\odot}$. There is already a suggestion in Fig. 10 that, despite the comparable observed absolute magnitudes of the RQQs and RLQs, the predicted Eddington luminosities of the RQQs are somewhat smaller. If the values of $m_{\rm bh}$ derived from $P^{\rm core}_{\rm 5\,GHz}$ are used to predict Eddington M_R, the difference becomes even more stark (as shown in Fig. 13), and shows that in selecting optically matched samples of RQQs and RLQs we may in fact have selected lower mass ($\simeq 10^9\,{\rm M}_{\odot}$) black holes radiating close to the

Eddington limit for comparison with higher mass ($\simeq 10^{10}\,M_\odot$) black holes radiating (in the optical) at around 10 per cent of their Eddington luminosity.

In summary, our results to date can be interpreted in two distinct ways, depending on whether $P^{\rm core}_{5\,\rm GHz}$ or host-galaxy luminosity is the more reliable predictor of black hole mass. If the former, then the difference between radio-loud and radio-quiet AGN may simply be that FRII radio sources require black holes of mass $m_{\rm bh} > 10^{10}\,M_\odot$. If the latter, then at least some of the RQQs in our sample would also appear to be powered by black holes with $m_{\rm bh} > 10^{10}\,M_\odot$, and some other explantion (e.g., black hole angular momentum) would be required to explain why black holes of comparable mass can produce radio sources which differ by two orders of magnitude in radio power, despite the fact that both are radiating in the optical with comparable efficiency.

Completion of our sample, coupled with proposed deeper radio observations of the undetected RQQs should assist in clarifying this issue.

6 CONCLUSIONS

In this paper we have presented and analysed the deep WFPC2 R675W images of the 19 objects (RGs, RLQs and RQQs) observed with the *HST* during the first year of our comparative *HST* imaging study of the host galaxies of luminous AGN. The results indicate that this carefully controlled study will, as hoped, be able to identify unambiguously the morphological type of the host galaxy of every AGN in our final 33-source sample. From the images analysed in this paper we find that the underlying hosts of *all three* classes of luminous AGN are massive elliptical galaxies, with scalelengths $\simeq 10$ kpc. Since the RQQ subsample is already close to completion, we can therefore for the first time state with some confidence that essentially all RQQs brighter than $M_R = -24$ reside in massive ellipticals, a result which removes the possibility that 'radio loudness' is directly linked to host-galaxy morphology.

The existence of comparably detailed modelling of deep *K*-band images of all the sources in our sample (Dunlop et al. 1993; Taylor et al. 1996) has allowed us to use our new *R*-band results to derive the first reliable optical–infrared colours for the hosts of a substantial sample of AGN. The preliminary results indicate that the hosts of all three classes of AGN have underlying stellar populations with ages comparable to that observed in normal, old ellipticals at similar redshift, despite the evidence for superimposed acivity arising from interactions/mergers. We also find that the distribution of host-galaxy axial ratios is consistent with that displayed by the normal elliptical galaxy population.

The RG and RLQ subsamples have been designed to be matched in terms of radio luminosity, radio spectral index, and redshift. Comparison of the host-galaxy properties of the (still small) RG and RLQ subsamples observed to date indicates that their hosts are indistinguishable in terms of morphological type, luminosity, axial ratio, and $R-K$ colour, consistent with unification via orientation.

The RQQ and RLQ samples were designed to be matched in terms of optical luminosity and redshift, and the image analysis presented here indicates that, with the exception of two low-luminosity interlopers in the RQQ sample (0257+024 and 2344+184, which should really be reclassified as Seyferts), the distributions of nuclear absolute magnitude for the RQQ and RLQ subsamples do indeed appear to be well matched. Interestingly, therefore, with the exception of 0257+024 and 2344+184, we find the host galaxies of the RQQs also to be massive elliptical galaxies, albeit approximately 0.5 mag fainter on average than their radio-loud counterparts. With the present subsamples this difference is not significant, but when the black hole mass in these quasars is inferred from the luminosity of their host spheroid, it implies that the typical black hole mass for the RQQs in our sample is $\simeq 7\times10^9\,M_\odot$, while for the RLQs it is $\simeq 15\times10^9\,M_\odot$, and that several of the luminous RQQs we have selected are radiating close to their Eddington limit (whereas very few of the RLQs appear to be radiating at more than $\simeq$10 per cent of predicted Eddington luminosity).

Finally, we find that the black hole mass estimates obtained from the luminosity of the host spheroid are in good agreement with independent estimates based on extrapolation of the relation between black hole mass and core radio luminosity established for nearby galaxies, and it seems hard to escape the conclusion that all the radio-loud AGN in our sample have black hole masses in excess of $10^{10}\,M_\odot$. However, if the latter relation is adopted as the most reliable estimator, we would conclude that our RQQ sample is even more biased towards objects emitting close to their Eddington limit, and contains no object powered by a black hole as massive as $10^{10}\,M_\odot$. If this is correct, then the physical origin of radio loudness ($P_{5\,\rm GHz} > 10^{24}\,{\rm W\,Hz^{-1}\,sr^{-1}}$) may simply be the presence of a black hole more massive than $10^{10}\,M_\odot$, and this relatively clean result may have been previously concealed from us by the selection effects involved in striving to produce a bright RQQ sample for comparison with a (radio-selected) RLQ sample, coupled with substantial scatter in the $m_{\rm bh}$: host-luminosity relation. Alternatively, if our values of $m_{\rm bh}$ derived from host-galaxy spheroid luminosity are more reliable, then at least some of the RQQs in our sample would have black hole masses $m_{\rm bh} > 10^{10}\,M_\odot$, comparable to RLQs, and some explanation other than simply black hole mass would still be required to account for the fact that the RLQs are two orders of magnitude more luminous at radio wavelengths. Completion of our *HST* study, coupled with deeper radio observations of the as-yet-undetected RQQs, should help to distinguish between these two alternative scenarios.

ACKNOWLEDGMENTS

Based on observations with the NASA/ESA *Hubble Space Telescope*, obtained at the Space Telescope Science Institute, which is operated by the Association of Universities for Research in Astronomy, Inc. under NASA contract No. NAS5-26555. This research has made use of the NASA/IPAC Extragalactic Database (NED) which is operated by the Jet Propulsion Laboratory, California Institute of Technology, under contract with the National Aeronautics and Space Administration. MJK acknowledges the award of a PPARC PDRA, and also acknowledges support for this work provided by NASA through grant numbers 00548 and 00573 from the Space Telescope Science Institute, which is operated by AURA, Inc., under NASA contract NAS5-26555. RJM acknowledges a PPARC studentship. DHH acknowledges the award of a PPARC PDRA.

REFERENCES

Akujor C. E., Spencer R. E., Zhang F. J., Davis R. J., Browne I. W. A., Fanti C., 1991, MNRAS, 250, 215

Antonucci R. R. J., 1985, ApJS, 59, 499

Bahcall J. N., Kirhakos S., Schneider D. P., 1994, ApJ, 435, L11
Bahcall J. N., Kirhakos S., Schneider D. P., 1995a, ApJ, 447, L1
Bahcall J. N., Kirhakos S., Schneider D. P., 1995b, ApJ, 450, 486
Bahcall J. N., Kirhakos S., Schneider D. P., 1996, ApJ, 457, 557
Bahcall J. N., Kirhakos S., Saxe D. H., Schneider D. P., 1997, ApJ, 479, 642
Barthel P. D., 1989, ApJ, 336, 606
Capaccioli M., Caon N., D'Onofrio M., 1992, MNRAS, 259, 323
Carballo R., Sánchez S. F., González-Serrano J. I., Benn C. R., Vigotti M., 1998, AJ, 115, 1234
De Koff S. et al., 1996, ApJS, 107, 621
Disney M. J. et al., 1995, Nat, 376, 150
Dunlop J. S., 1997, in Bremer M. et al., eds, Observational Cosmology with the New Radio Surveys. Kluwer, Dordrecht, p. 157
Dunlop J. S., 1999, in Rottgering H. J. A., Best P., Lehnert M. D., eds, The Most Distant Radio Galaxies, KNAW Colloquium Amsterdam. Kluwer, Dordrecht, p. 71
Dunlop J. S., Taylor G. L., Hughes D. H., Robson E. I., 1993, MNRAS, 264, 455
Ellingson E., Yee H. K. C., Green R. F., 1991, ApJ, 371, 41
Fabian A. C., Rees M. J., 1995, MNRAS, 277, L55
Feigelson E. D., Isobe T., Kembhavi A., 1984, AJ, 89, 1464
Franceschini A., Vercellone S., Fabian A. C., 1998, MNRAS, 297, 817
Giovannini G., Feretti L., Gregorini L., Parma P., 1988, A&A, 199, 73
Glazebrook K., Peacock J. A., Miller L., Collins C. A., 1995, MNRAS, 275, 169
Gower A. C., Hutchings J. B., 1984a, PASP, 96, 19
Gower A. C., Hutchings J. B., 1984b, AJ, 89, 1658
Guiderdoni B., Rocca-Volmerange B., 1987, A&A, 186, 1
Haehnelt M. G., Rees M. J., 1993, MNRAS, 263, 168
Heckman T. M., Bothun G. D., Balick B., Smith E. P., 1984, AJ, 89, 958
Heckman T. M. et al., 1986, ApJ, 311, 526
Hooper E. J., Impey C. D., Foltz C. B., 1997, ApJ, 480, L95
Hughes D. H., Kukula M. J., Dunlop J. S., Boroson T. B., 1999, MNRAS, submitted
Hutchings J. B., 1995, Nature News & Views, 376, 118
Hutchings J. B., Morris S. C., 1995, AJ, 109, 1541
Hutchings J. B., Neff S. G., 1992, AJ, 104, 1
Hutchings J. B., Neff S. G., 1997, AJ, 113, 550
Hutchings J. B., Johnson I., Pyke R., 1988, ApJS, 66, 361
Hutchings J. B., Janson T., Neff S. G., 1989, ApJ, 342, 660
Hutchings J. B., Holtzman J., Sparks W. B., Morris S. C., Hanisch R. J., Mo J., 1994, ApJ, 429, L1
Kormendy J., Richstone D., 1995, ARA&A, 33, 581
Kotilainen J. K., Ward M. J., 1994, MNRAS, 266, 953
Kukula M. J., Dunlop J. S., Hughes D. H., Rawlings S., 1998, MNRAS, 297, 366
Kukula M. J. et al., 1997, in Clements D. L., Pérez-Fournon I., eds, Quasar Hosts, Proc. ESO/IAC conference. Springer-Verlag, Berlin, p. 177
Leahy J. P., Pooley G. G., Riley J. M., 1986, MNRAS, 222, 753
Lin H., Kirshner P. P., Schectman S. A., Landy S. D., Oemler A., Tucker D. L., Schechter P. L., 1996, ApJ, 464, 60
Lister M. L., Gower A. C., 1994, AJ, 108, 821
MacKenty J. W., 1990, ApJS, 72, 231
McCarthy P. J., van Breugel W., Kapahi V. K., 1991, ApJ, 371, 478
McLeod K. K., Rieke G. H., 1994a, ApJ, 420, 58
McLeod K. K., Rieke G. H., 1994b, ApJ, 431, 137
McLeod K. K., Rieke G. H., 1995a, ApJ, 441, 96
McLeod K. K., Rieke G. H., 1995b, ApJ, 454, L77
McLure R. J. et al., 1999, MNRAS, submitted
Magorrian J. et al., 1998, AJ, 115, 2285
Miley G. K., Hartsuijker A. P., 1978, A&AS, 34, 129
Miller P., Rawlings S., Saunders R., 1993, MNRAS, 263, 425
Peacock J. A., 1987, in Kundt W., ed., Astrophysics Jets and Their Engines. Reidel, Dordrecht, p. 185
Romney J. et al., 1984, A&A, 135, 289
Ryden S., 1992, ApJ, 396, 445
Sandage A. R., Freeman K. C., Stokes N. R., 1970, ApJ, 160, 831
Schneider D. P., Gunn J. E., Hoessel J. G., 1983, ApJ, 268, 476
Silk J., Rees M., 1999 8, A&A, 331, L1
Small T. A., Blandford R. D., 1992, MNRAS, 259, 725
Smith E. P., Heckman T. M., 1990, ApJ, 348, 38
Smith E. P., Heckman T. M., Bothun G. D., Romanishin W., Balick B., 1986, ApJ, 306, 64
Stockton A., Farnham T., 1991, ApJ, 371, 525
Taylor G. T., Dunlop J. S., Hughes D. H., Robson E. I., 1996, MNRAS, 283, 930
Trauger J. T. et al., 1994, ApJ, 435, L3
Turnshek D. A., Bohlin R. C., Williamson R., Lupie O., Koornneef J., Morgan D., 1990, AJ, 99, 1243
Urry C. M., Padovani P., 1995, PASP, 107, 803
van Breugel W., Miley G., Heckman T., 1984, AJ, 89, 5
Véron-Cetty M. P., Woltjer L., 1990, A&A, 236, 69
Véron-Cetty M. P., Woltjer L., Roy A. L., 1991, A&A, 246, L73
Young S. et al., 1998, MNRAS, 294, 478

APPENDIX A: THE IMAGES

The images, two-dimensional model fits, and model-subtracted residual images. A grey-scale/contour image of the final reduced F675W *R*-band image of each AGN is shown in the top-left panel (panel A) of each of Figs A1–A19, which shows a region $12.5 \times 12.5\,\mathrm{arcsec}^2$ centred on the target source. The surface brightness of the lowest contour level is indicated in the top-right corner of the panel with the grey-scale designed to highlight structure close to this limit. Higher surface brightness contours are spaced at intervals of $0.5\,\mathrm{mag\ arcsec}^{-2}$, and have been superimposed to emphasize brighter structure in the centre of the galaxy/quasar. Panel B in each figure shows the best-fitting two-dimensional model, complete with unresolved nuclear component (after convolution with the empirical PSF) contoured in an identical manner to panel A. Panel C shows the best-fitting host galaxy as it would appear if the nuclear component were absent, while panel D is the residual image which results from subtraction of the full two-dimensional model (in panel B) from the raw *R*-band image (in panel A), in order to highlight the presence of morphological peculiarities such as tidal tails, interacting companion galaxies, or secondary nuclei. All panels are displayed using the same grey-scale.

This paper has been typeset from a TEX/LATEX file prepared by the author.

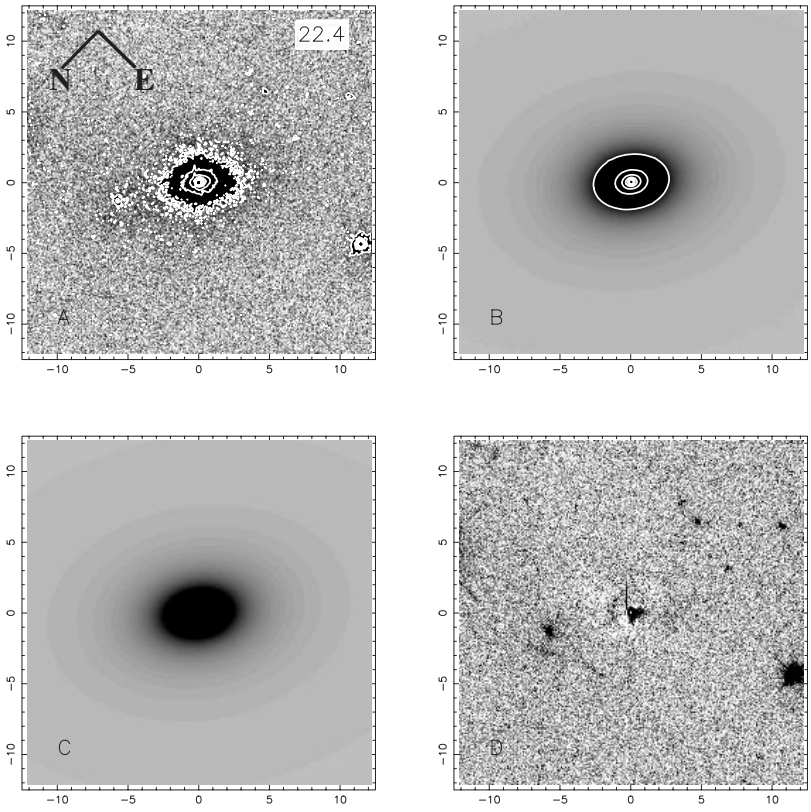

Figure A1. The radio galaxy 0345+337.

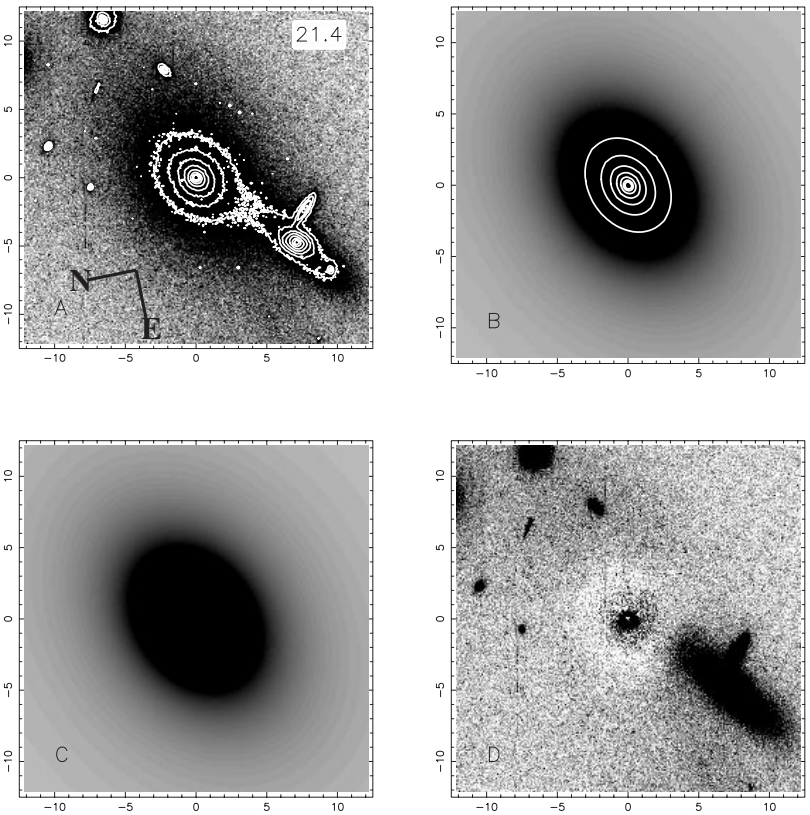

Figure A2. The radio galaxy 0917+459.

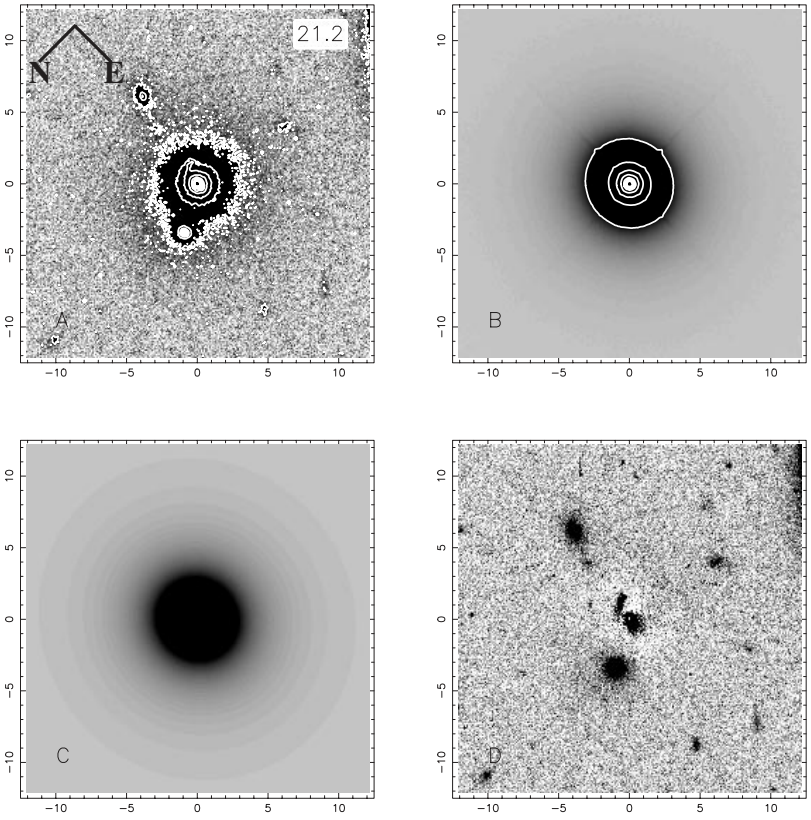

Figure A3. The radio galaxy 0958+291.

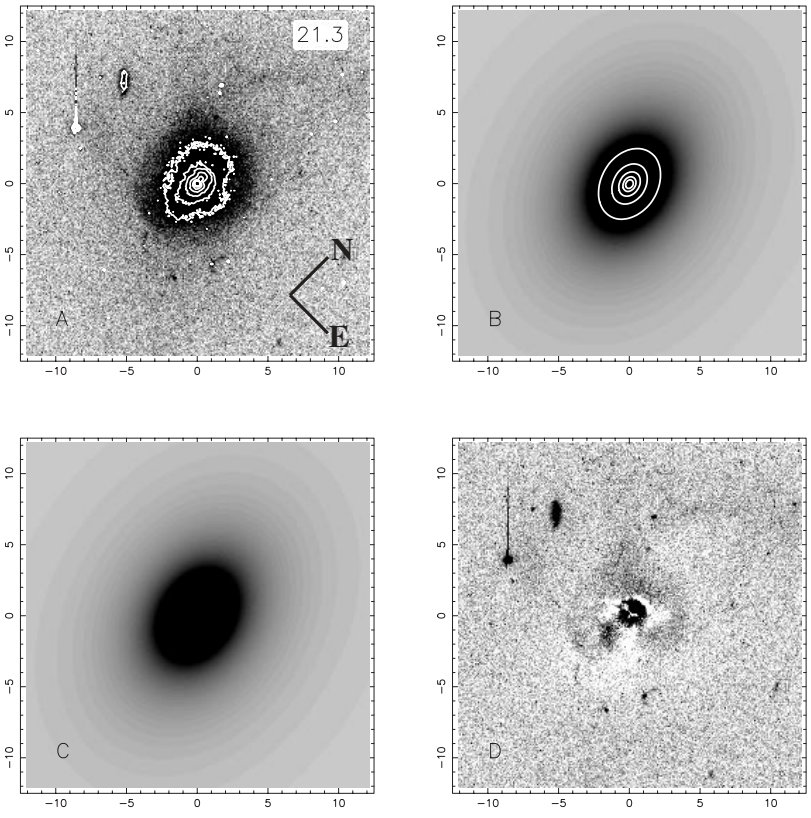

Figure A4. The radio galaxy 2141+279.

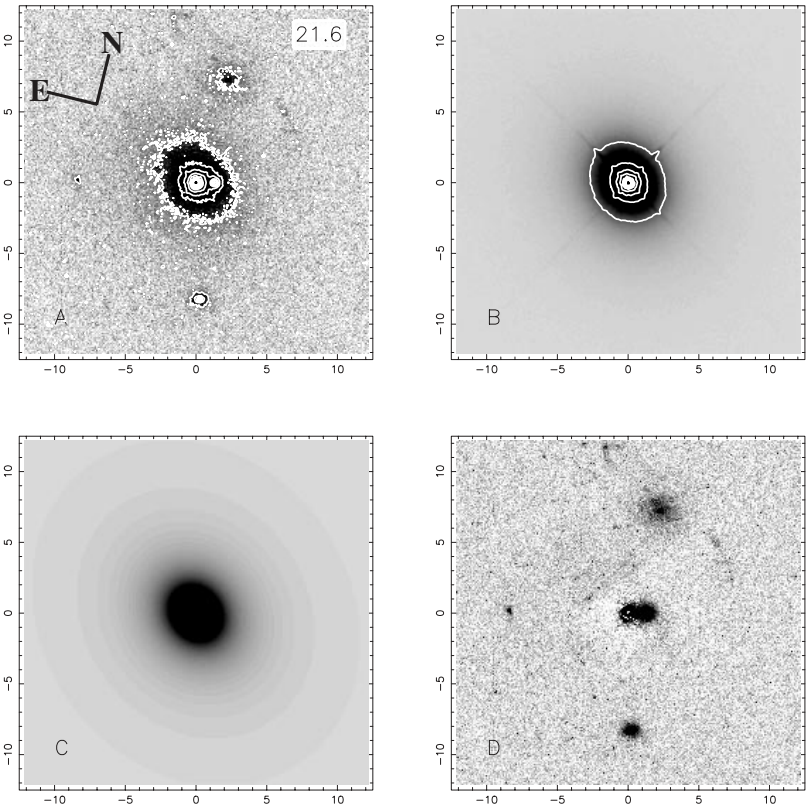

Figure A5. The radio-loud quasar 0137+012.

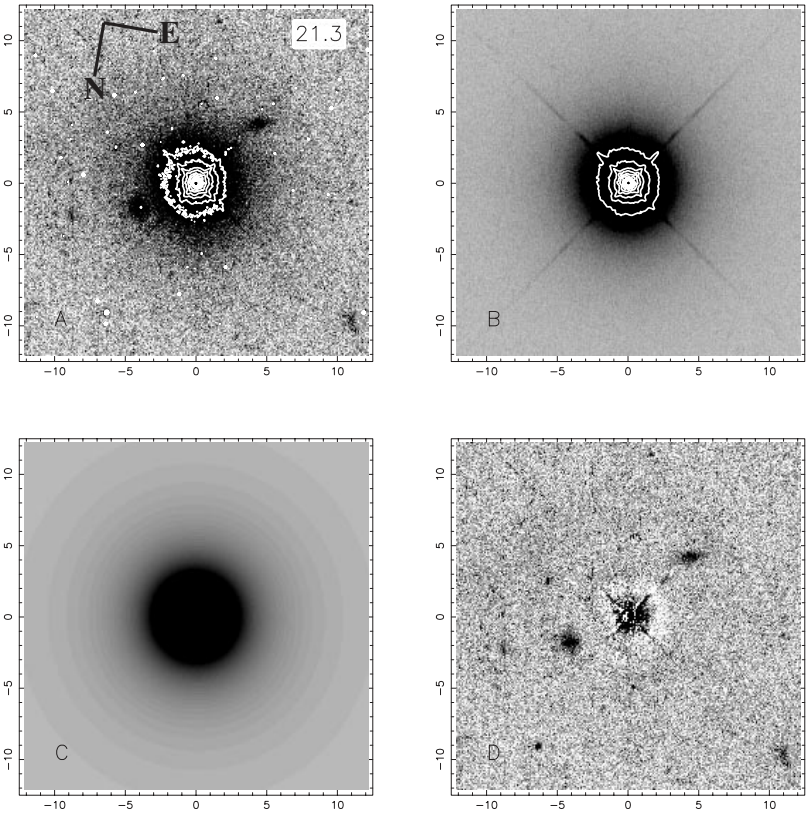

Figure A6. The radio-loud quasar 0736+017.

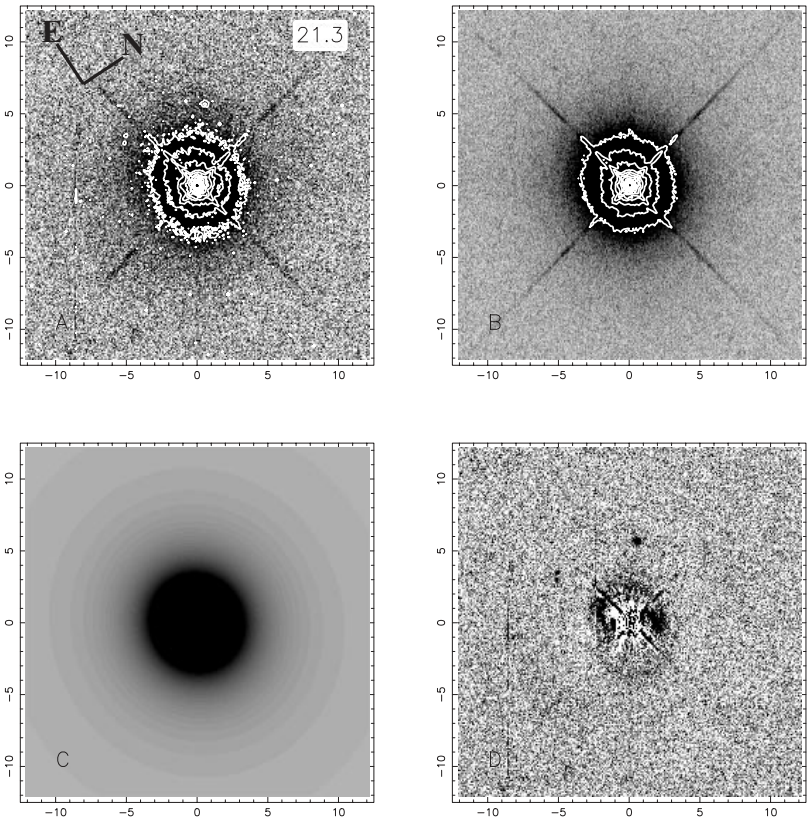

Figure A7. The radio-loud quasar 1004+130.

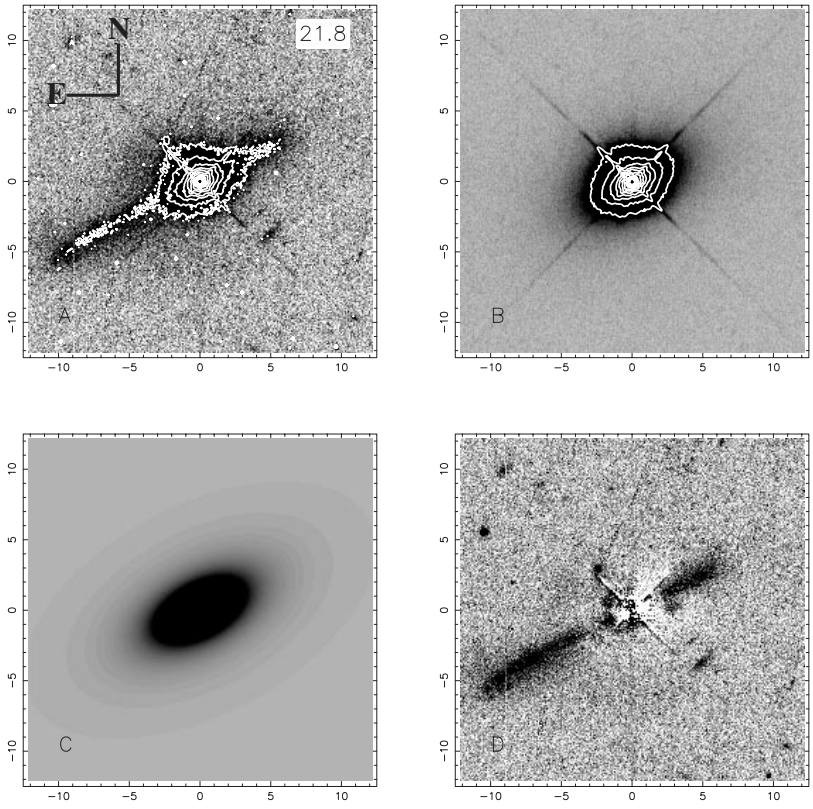

Figure A8. The radio-loud quasar 2141+175.

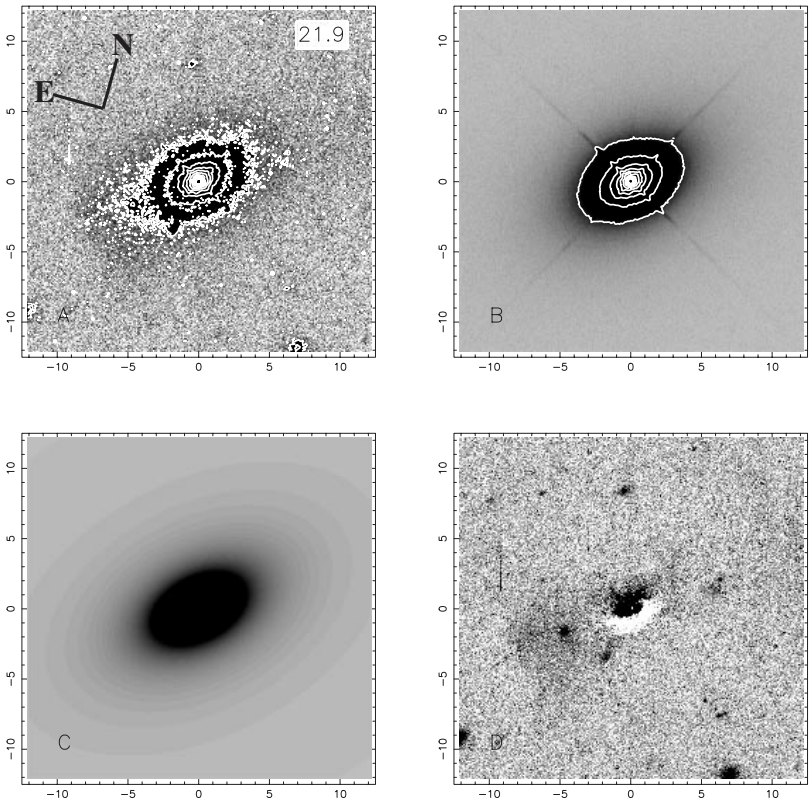

Figure A9. The radio-loud quasar 2247+140.

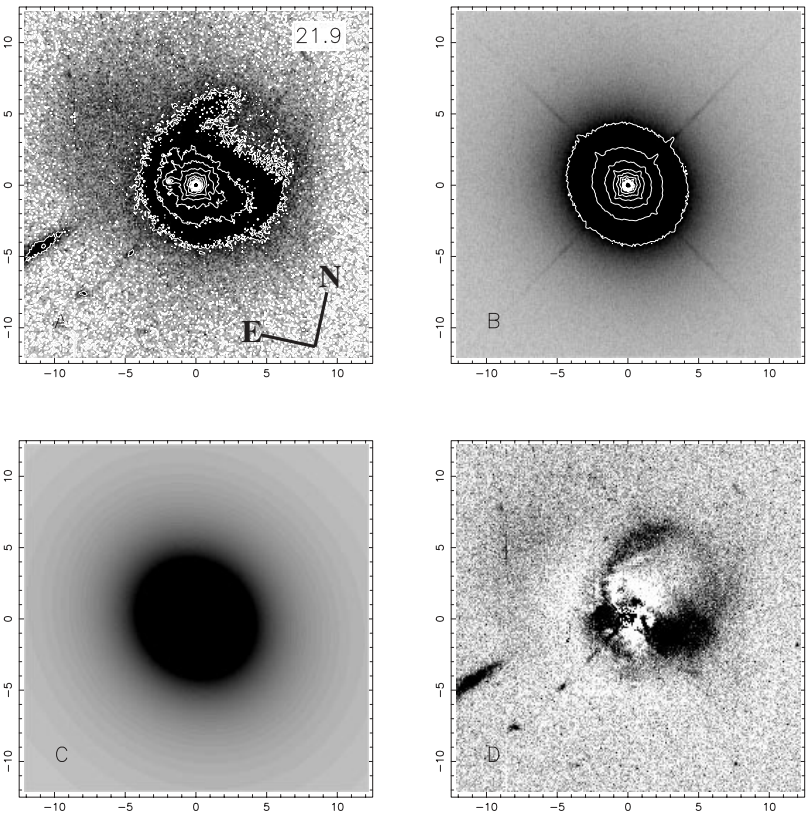

Figure A10. The radio-loud quasar 2349+014.

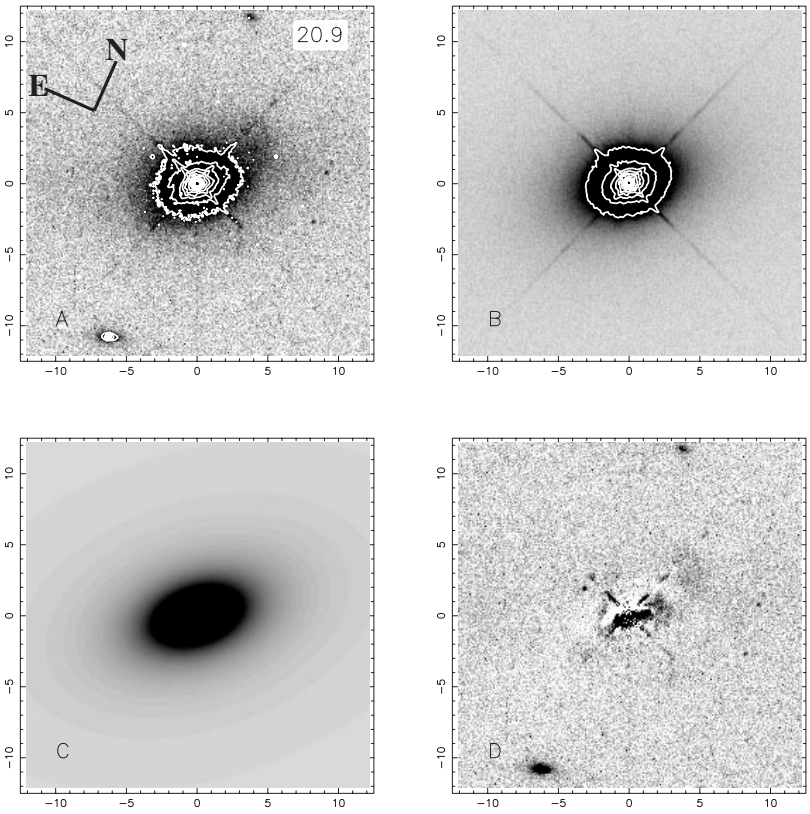

Figure A11. The radio-quiet quasar 0054+144.

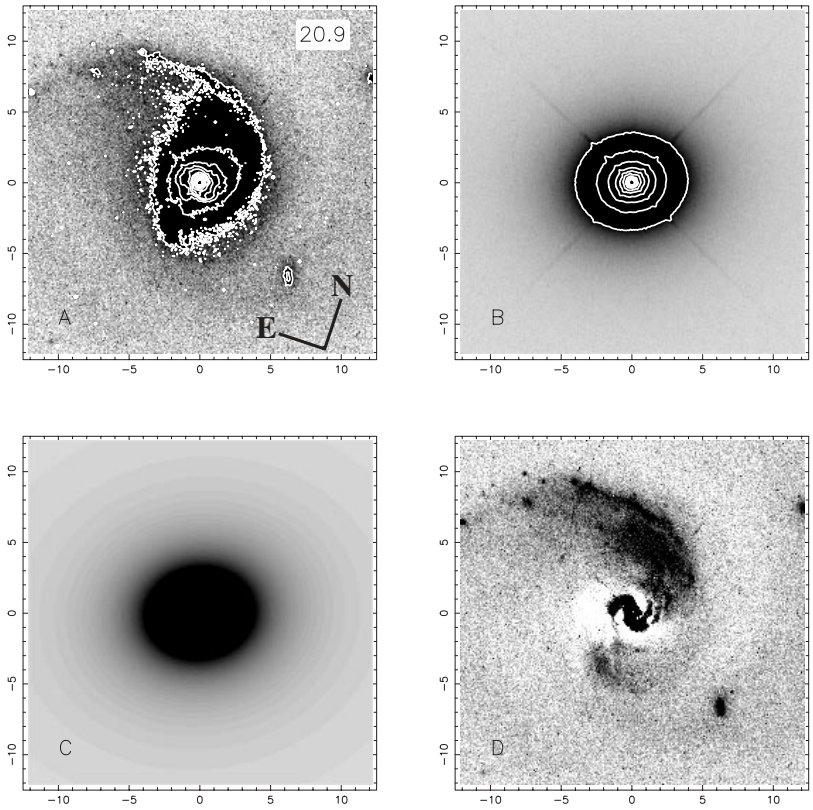

Figure A12. The radio-quiet quasar 0157+001.

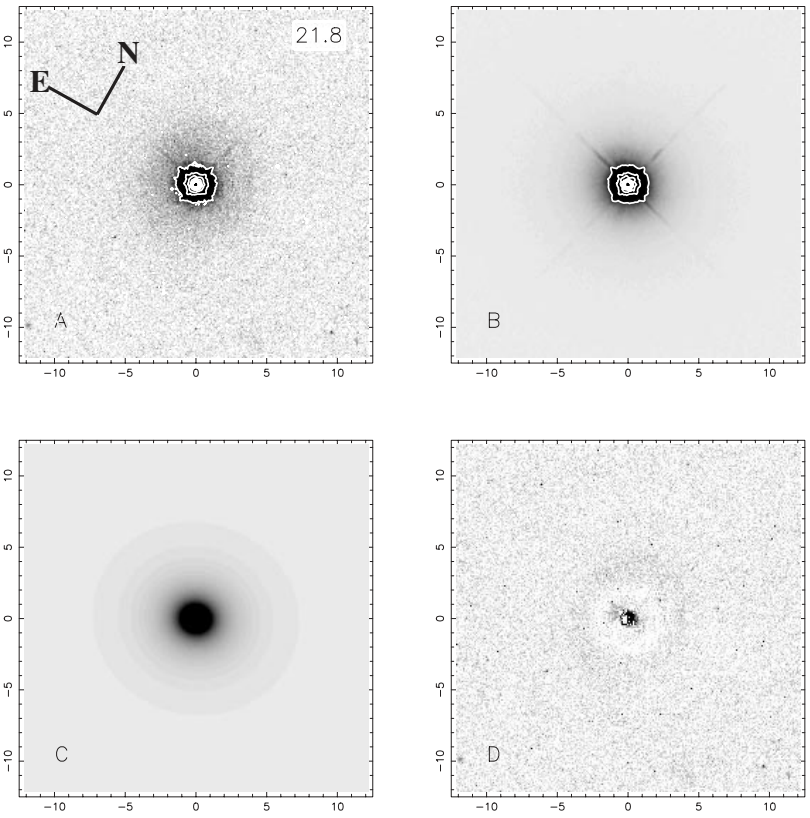

Figure A13. The radio-quiet quasar 0244+194.

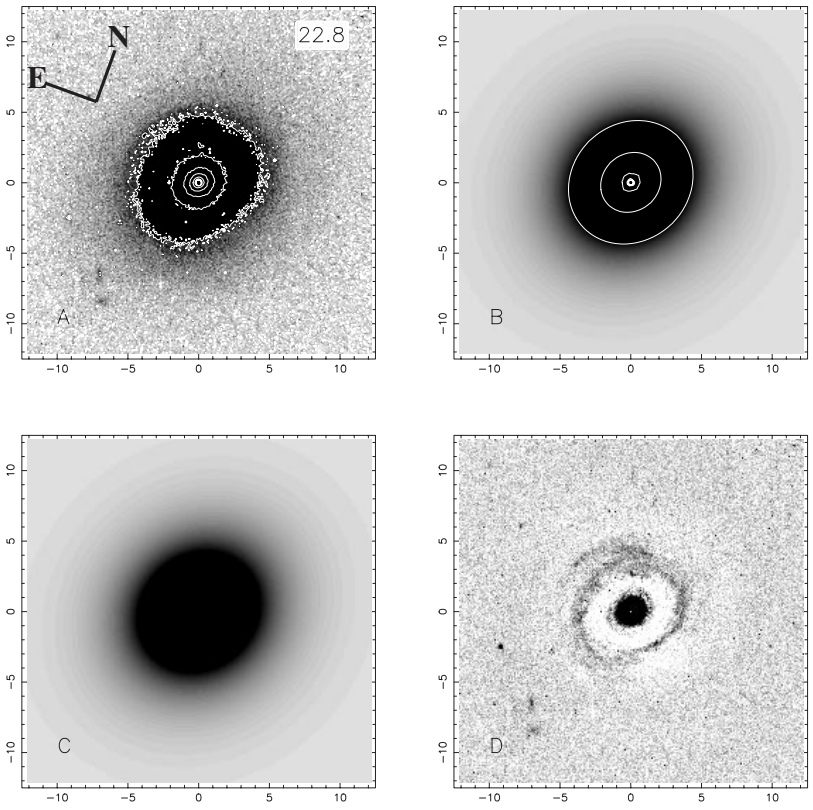

Figure A14. The radio-quiet quasar 0257+024.

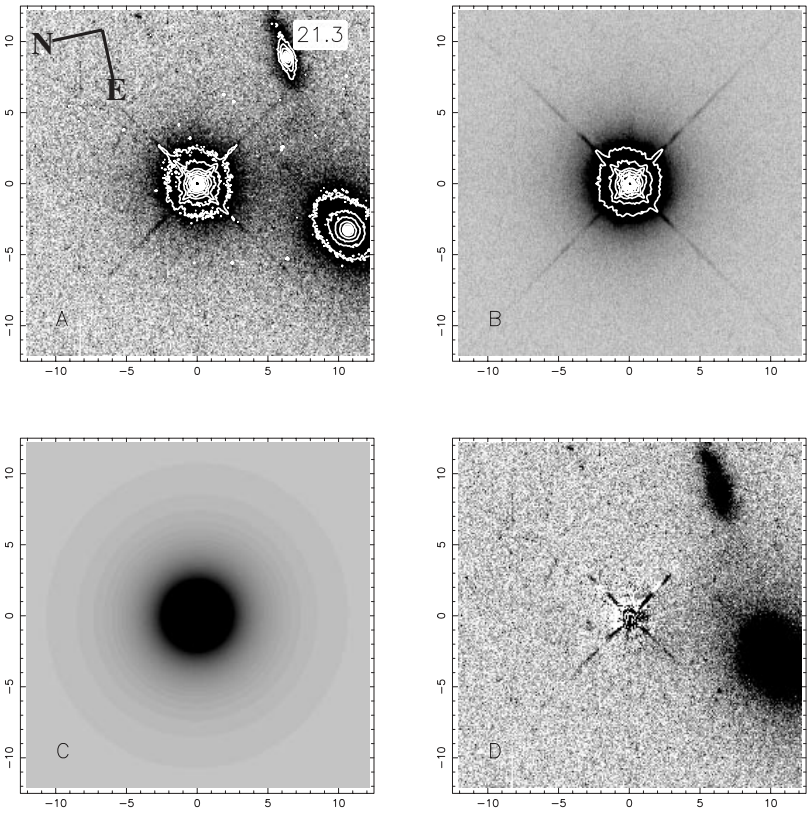

Figure A15. The radio-quiet quasar 0923+201.

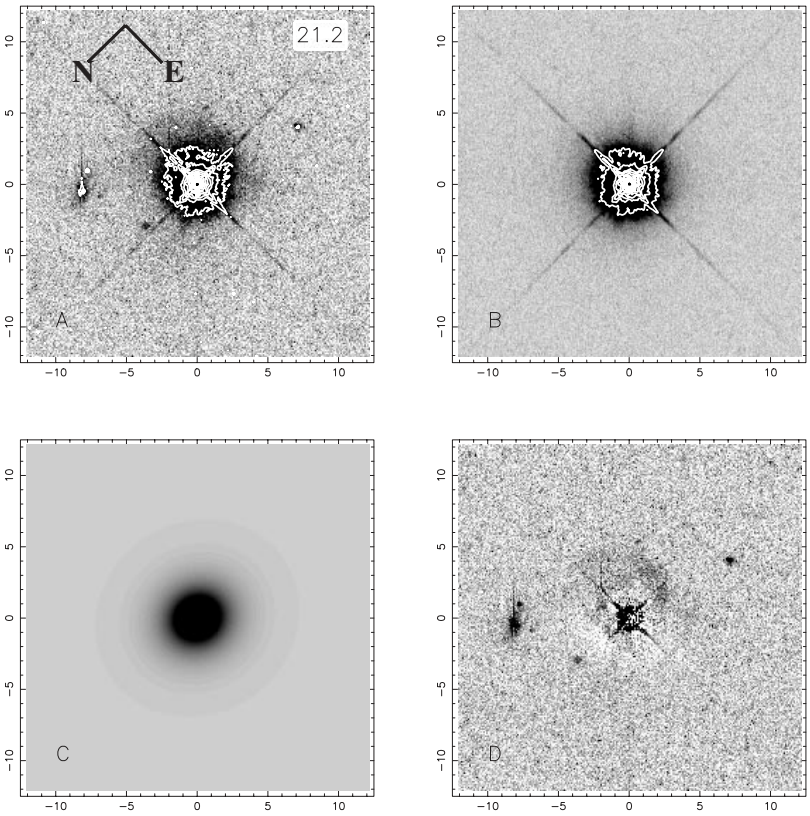

Figure A16. The radio-quiet quasar 0953+415.

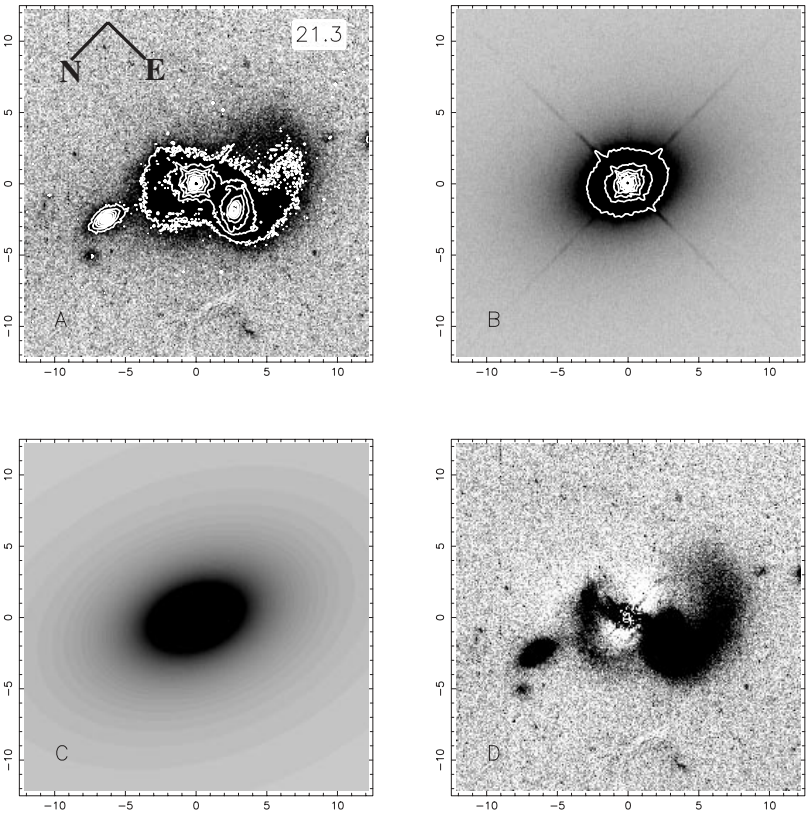

Figure A17. The radio-quiet quasar 1012+008.

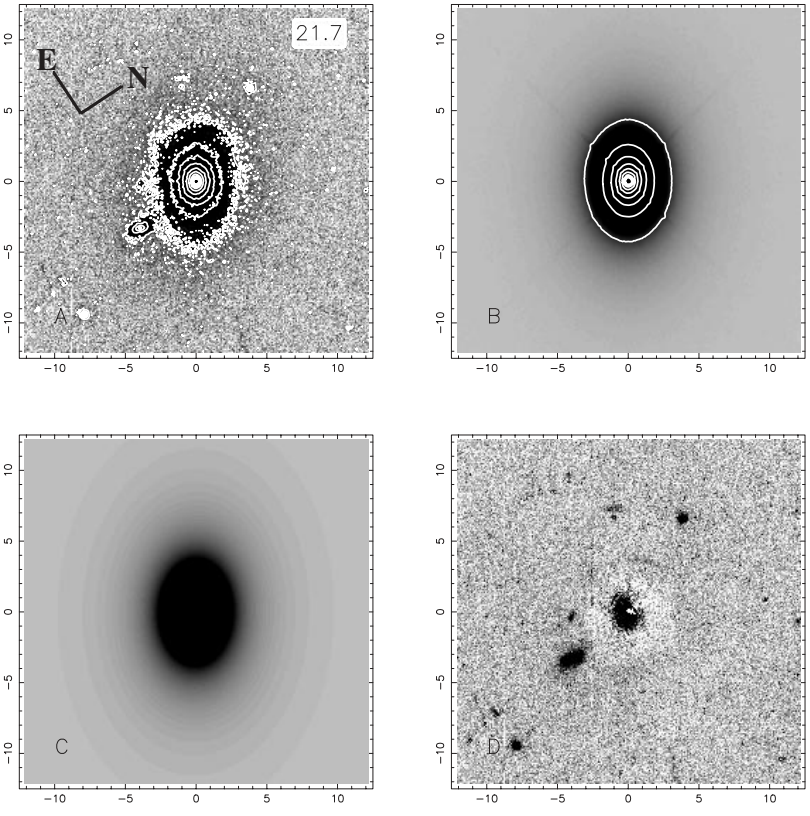

Figure A18. The radio-quiet quasar 1635+119.

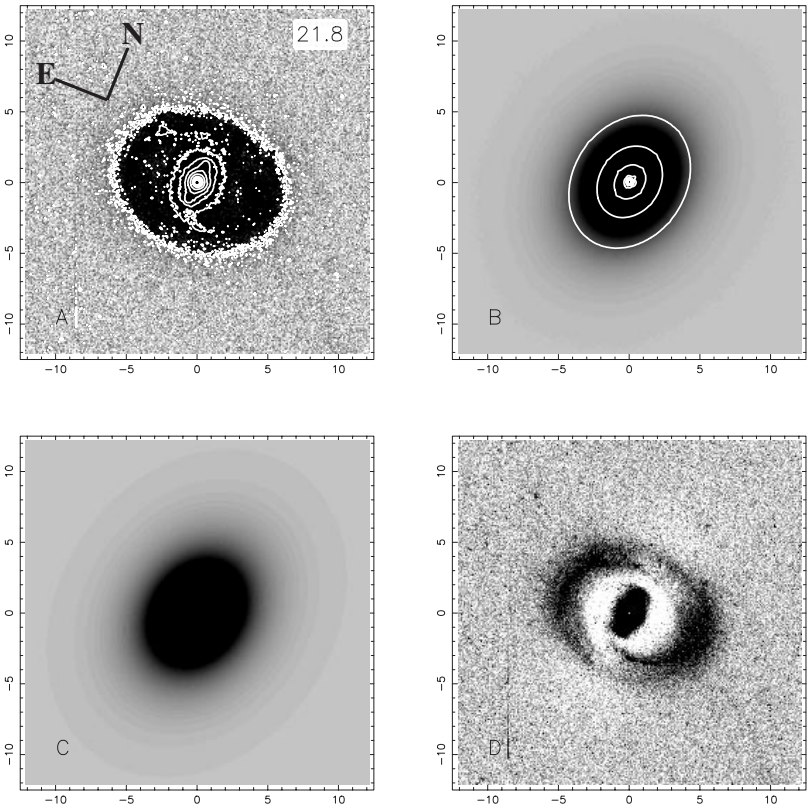

Figure A19. The radio-quiet quasar 2344+184.